Unravelling the evolution of an Allier river terrace

Combining Optically Stimulated Luminescence dating and tracing with Landscape Evolution Model LAPSUS for determining the evolution of the Allier catchment (Central Massif, France) during formation of terrace level Fx_{III}.

Monique T.C.M. Voesten
(960221900040)

MSc *Earth and Environment*
Specialisation:
Soil Geography and
Earth Surface Dynamics

MSc Thesis, June 2019

Supervisors:
Tony Reimann
Jeroen Schoorl

WAGENINGEN
UNIVERSITY & RESEARCH

Photo on front page: Sampling location of Allier Fx_{III} terrace, by Anna Broers

Unravelling the evolution of an Allier river terrace
Combining Optically Stimulated Luminescence dating and tracing with Landscape Evolution Model LAPSUS for determining the evolution of the Allier catchment (Central Massif, France) during formation of terrace level Fx_{III}.

Monique Theodora Cornelia Maria Voesten, June 2019
Registration number: 960221-900-040
SGL-80436
MSc-thesis Earth and Environment
Specialisation Soil Geography and Earth Surface Dynamics
Wageningen University

Supervisors:
Dr. T. Reimann
Dr. J.M. Schoorl
Examiner:
Dr. J.M. Schoorl

Chairgroup Soil Geography and Landscape
Phone: +31 317 482024
office.sgl@wur.nl

Postal address:
Postbus 47
6700 AA, Wageningen
The Netherlands

Visiting address:
Gaia (building number 101)
Droevendaalsesteeg 3
6708 PB, Wageningen
The Netherlands

Preface

This report is the result of my MSc thesis for the master Earth and Environment at Wageningen University and Research. Before going to the actual report, I would like to thank a few people who have helped me through my thesis:
First of all I would like to thank Tony Reimann and Jeroen Schoorl for providing this topic, which I really have enjoyed. Their enthusiasm every time when I came with new results gave me a boost to work further on my research. A special thanks to Jeroen for the help with LAPSUS and to Tony for the hours discussing my OSL data, which changed a lot through the process of this thesis.
I also would like to thank Tom Veldkamp for his valuable input and for his knowledge on the Allier area. Furthermore I greatly thank Alice Versendaal and Erna Voskuilen for their help in the NCL laboratory and for the occasional chat. Last but not least, I would like to thank my fellow MSc students who worked in the same office as me for the fun breaks we took and the nice atmosphere in the office, it helped me staying motivated till the end of my thesis!

Abstract

River terraces are archives of the landscape. Indications of climate change, tectonic activity and avulsions can all be present in the river terraces. The Allier river, located in the Limagne rift valley in the Central Massif, France, has a well-researched terrace staircase, but the evolution of the catchment during formation of some of the terrace levels remains unclear. One of these terrace levels, Fx_{III}, is recognisable by its darker coloured alluvial sediments due to basaltic material. In contrast with former research, this study looks at the longitudinal differences within one terrace level, to determine when and how the river landscape of the Allier catchment evolved during the formation of terrace level Fx_{III}.

Six samples of the Fx_{III} terrace are studied with Optically Stimulated Luminescence (OSL) dating and tracing techniques, using quartz Single Grain OSL and feldspar SG post-IR IRSL measurements. The Landscape Evolution Model LAPSUS was used to complement the OSL data, by determining where erosion and sedimentation took place. The OSL dating resulted in an average age of 16.9 ka, with individual samples ranging from 15.4-18.7 ka. This age can be linked to multiple volcanic eruptions within the Allier catchment. Furthermore, a decrease in quartz OSL sensitivity was found downstream and the amount of bleaching was similar for all six samples. LAPSUS showed that two sub catchments provide the most sediment to the Allier river, one in the southwest sandstone area and one in the northeast granite area. These areas provide an explanation for the decrease in OSL sensitivity: the upstream samples are affected by the sensitive sandstone sediments, while the downstream samples are affected by insensitive granites and saprolites from the eastern rift shoulder. The change in transport distance between the source areas and the sampling locations also can have an influence on the sensitivity. Furthermore, both a change in river dynamics and the change in sensitivity combined with a similar amount of bleaching for all samples indicates that bleaching might not happen in transport, but on erosional slopes or after deposition.

Contents

1. Introduction

River terraces are important archives for landscape evolution. Different than erosive landforms, terraces have registered a separate or completed era of aggradation in their sediments. Examples of processes that can be traced in the sediments of fluvial terraces are climate change, tectonics, sea level rise and fall, piracy of rivers and avulsions (e.g. Boenigk, 1995; Harmand & Cordier, 2012; Litchfield & Clark, 2015). To understand the evolution of the landscape, the terraces should be dated properly, which can be done with multiple techniques. Organic rich sediments and pieces of charcoal can be dated with ^{14}C-dating (Veldkamp & Kroonenberg, 1993; Berendsen & Stouthamer, 2000) and when tephra layers are present these can be dated with ^{14}C as well (Eden et al., 2001). Travertines, limestone formations deposited by (hot) springs, can be dated with Uranium Thorium decay series (Veldkamp & Kroonenberg, 1993). Other examples of dating methods which are useful for uncovering landscape evolution are Potassium-Argon dating on volcanic material (lava flows, basalts (Armstrong et al., 1975)), pollen (Taylor et al., 1994) and Optically Stimulated Luminescence (OSL) on quartz or feldspar minerals (Wallinga, 2002).

The Allier river is presumably one of the best researched showcases for river evolution providing a long research history (Pastre, 1987, 2004, 2005; T. Veldkamp, 1991; Broers MSc thesis, 2016). The Allier is a large tributary of the Loire, located in the Massif Central, France (figure 1). The Allier has a length of 410 kilometres and has several tributaries of its own, of which the Dore, which confluences in between the measurement points shown in figure 1, is the largest one.
The Allier river drains the Limagne rift valley, which is filled with Oligocene clays, marls and sandstones, and part of the western and eastern rift shoulders, with Hercynian basement system plutonic and high metamorphic rocks, dominantly granites. In addition the western rift shoulder is covered and influenced by Miocene, Pliocene and Quaternary volcanics, see figure 1 (Cubizolle et al., 2001; Lucazeau et al., 1984). Lava flows, which are often basaltic, from old eruptions run from the rift shoulder into the graben. Due to their low erosivity they are preserved in the landscape.

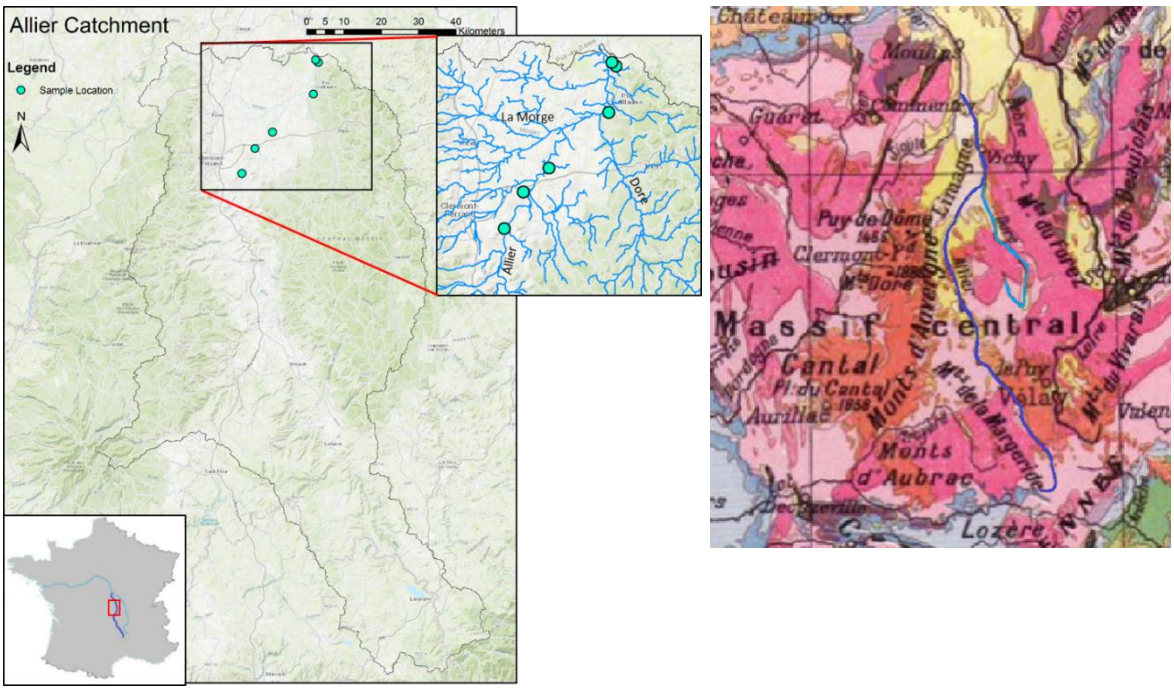

Figure 1. Left: Allier Catchment (dark blue), a tributary of the Loire (light blue). Located in the Massif Central, France. Two tributaries and sampling locations from terrace level Fx_{III} are indicated (Dore and La Morge). Order of samples upstream to downstream (from south to north): NCL-2515 -177, -182, -180, -190, -188 and -187. Right: Geological map of the Massif Central. Reddish colour indicates volcanics, yellow indicates Oligocene sediment infill. Light pink indicates granites and dark pink indicates the Hercynian basement. The Allier river is the dark blue and the Dore the light blue line.

The Allier river has an extensive terrace staircase dating back from early Pleistocene till Holocene deposits (Pastre, 2005). The terrace staircase is coded in French literature from Fz (current floodplain) till Ft (>2 Ma) (Pastre, 2005), as shown in figure 2 (Veldkamp & Kroonenberg, 1993; Pastre, 2005; Veldkamp et al., 2016). The youngest terrace levels (z, y, x, and w, figure 2) are dated with ^{14}C (on travertines and organic rich sediments), U/Th (on travertines) and OSL (on quartz and feldspar minerals) (Veldkamp, 1991; Broers, 2016; unpublished NCL report). In the past,

subdivisions were made within the terrace levels to distinguish between different aggradational phases, for example Fw_a and Fw_b. For the late Pleistocene terrace level Fx this is even further debated: it can be subdivided in morphological units Fx_a and Fx_b, but also in lithostratigraphical units Fx_I, Fx_{II}, Fx_{III} and Fx_{IV} (figure 2) (Veldkamp & Kroonenberg, 1993).
This research focusses on terrace level Fx_{III}. This terrace level can be recognised for its darker appearance compared to other terrace levels, resulting from a high percentage of dark minerals most probably of volcanic, basaltic origin (Veldkamp & Kroonenberg, 1993). This material is dominantly produced and found on the western rift shoulder throughout the Late Quaternary.

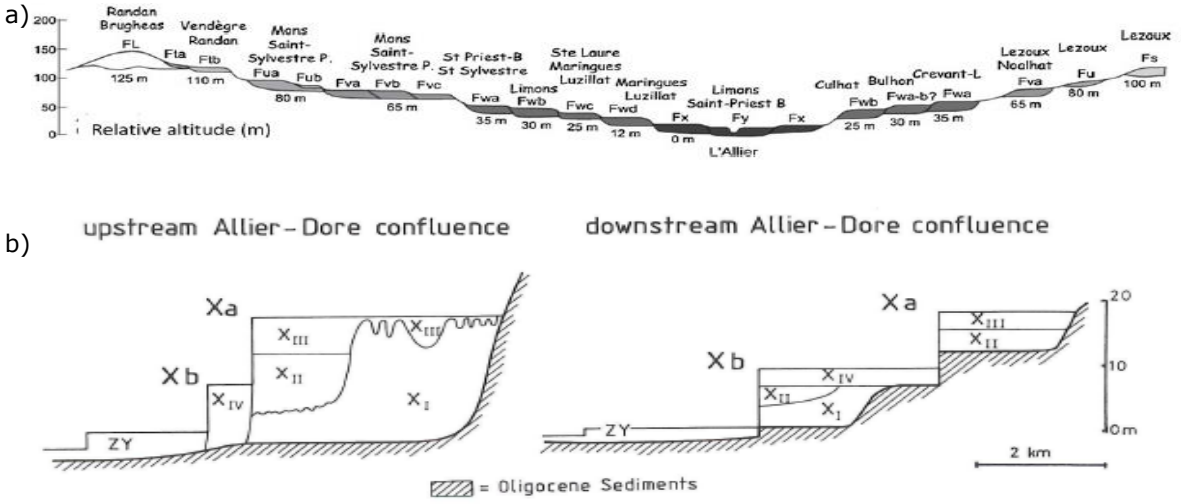

Figure 2. a) Terrace staircase of the Allier river (Pastre, 2005); b) Morphology and schematical lithostratigraphy Fx terrace level (Veldkamp & Kroonenberg, 1993). Upstream terrace level FxIII overlies cryoturbated soils of the FxI terrace layer. Downstream terrace level FxIV can be found, which is also rich in volcanic material, but lies on a lower level (Veldkamp & Kroonenberg, 1993).

Previous research investigated the burial age of the alluvial sediments associated to this terrace level (Broers MSc thesis 2016; unpublished NCL report) (figure 3). The result of this dating infers younger ages of burial-deposition stream upwards, which is uncommon, and the spread in between measurements is large. The OSL dates also do not agree with the expected age of this terrace based on ^{14}C-dating of charcoal and organic lacustrine sediments from a nearby marais (Veldkamp & Kroonenberg, 1993). The Fx_{III} terrace is thought to be coeval with the formation of the lake sediments, because both the lacustrine sediments and the Fx_{III} terrace are intercalated between a Middle Pleniglacial cryoturbated surface and an Allerød trachy-andesitic ash (Veldkamp & Kroonenberg, 1993).

Usually multiple stacked terrace levels are dated to establish a conventional chronostratigraphy (Veldkamp, 1991; Pastre, 2005; Schumm, 1993). In this research the longitudinal profile of only one terrace level is studied, to investigate the temporal and process related uniformity. This can provide information on the processes leading to terrace formation. In the case of terrace level Fx_{III} the change in age to the downstream part raises questions. It could mean that aggradation of the terrace happened in multiple events, while till now it is assumed to be of one age and thus originating from only one aggradational event (Broers MSc thesis, 2016).
In the case of a single event and considering the age as found by Broers (2016) and NCL (Nederlands Centrum van Luminescentie), it would mean that the aggradation phase started downstream and the upstream part of the catchment responded later to for example climatic change, which makes it a diachronous aggradation event (Bull, 1990). In the case of multiple aggradation events it might be that the ages are correct, but that the terraces in the two locations were built up during two different events, for example volcanic eruptions. According to Nowell et al. (2006) volcanic events happen in clusters, so it might be possible that multiple eruptions are the cause for the formation of the terrace level. Since the assumed age of the terrace is still within the ice age, this could have provoked rapid melting of ice sheets overlapping the volcanoes, which could transport large amounts of volcanic (basaltic) material to the Allier river. Another possibility would be mixing with older tributary sediments. Tributary sediments can seem older than the main river sediments due to differences in signal resetting (see *Chapter 2.1*, OSL page 9) because of differences in turbidity (López et al., 2018). When the sediments from the tributary are not fully reset and still get deposited together with the younger sediments from the main river, it will influence the dating of these terrace sediments. If this is the case, it would mean that the ages downstream are probably overestimated.

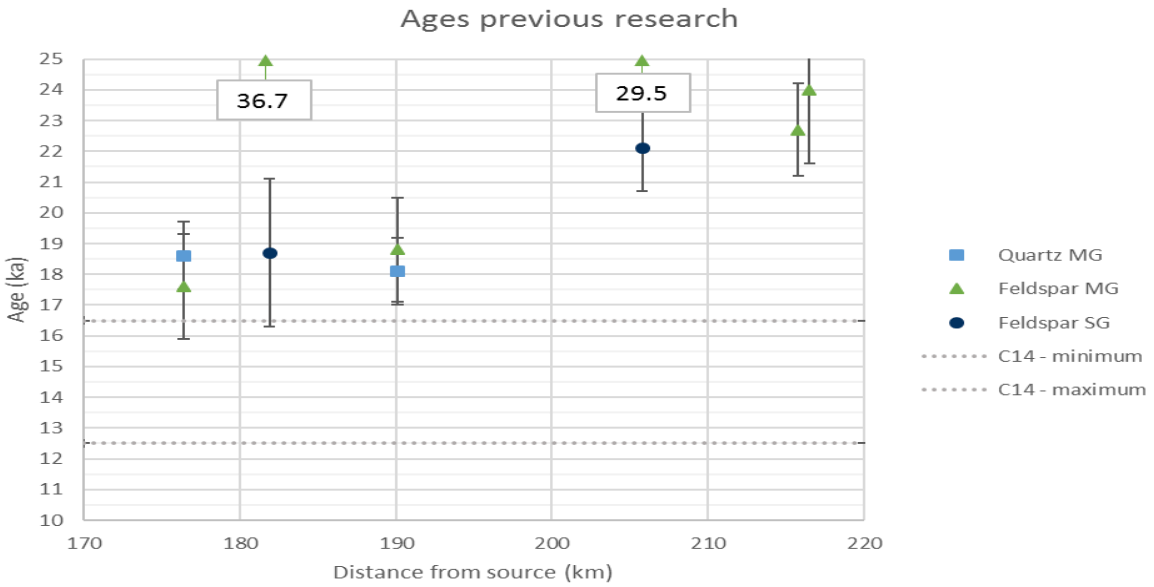

Figure 3. Ages of samples of the FxIII terrace from previous research. The X-axis shows the distance from the source of the Allier river. A table of these ages can be found in the appendix (A1). MG = multiple grain OSL measurement, SG = single grain OSL measurement. The numbered boxes show two ages found with MG feldspar measurements, but due to readability reasons these are not plotted.

To summarize, the following hypotheses are considered for the formation of the Fx_{III} terrace of the Allier river:

A) Synchronous terrace development, due to multiple events (e.g. volcanic eruptions).
B) Synchronous terrace development, due to a single event (e.g. tributary mixing).
C) Diachronous terrace development, due to a single event (e.g. climate change).

Since OSL measurements will probably not be enough to deduce which hypothesis will most likely be true, Landscape Evolution Models (LEMs) will be used in this study to complement the OSL data. These models show where erosion and sedimentation takes place on the basis of a digital elevation model. In the LEM LAPSUS (Landscape process modelling at multi-dimensions and scales (Schoorl, Sonneveld, & Veldkamp, 2000) one can change the forcing, such as the intensity or length of rainfall events, to simulate climatic conditions. The combination of LEMs and OSL has to my knowledge not been done before. This new approach will be useful to derive where the sediments occurring in the terrace originate and whether the terrace can be related with certain events or not.

1.1 Research objectives

Some of the ages as presented by Broers (2016) and NCL are doubtful or questionable (appendix A1). Therefore the first objective of this research is to improve the chronology for the Allier river terrace level Fx_{III}. Next to that, I will use different OSL techniques in combination with the LEM LAPSUS to better constrain river landscape dynamics. The tracing techniques using OSL will provide information on sediment transport in the Allier, on the possible source of the sediments and on the transport distance (Pietsch et al., 2008; Reimann et al., 2015; López et al., 2018). The LEM will contribute to this by providing the source areas and showing which areas contribute most to the sediment supply to the Allier river (Schoorl, Sonneveld & Veldkamp, 2000). This knowledge is needed to understand the evolution of the Allier catchment at the time of the Fx_{III} terrace level deposition.

The renewed dating of the terrace will be complemented with a new OSL approach called tracing. I will use the following three OSL tracing techniques:

1) Bleaching rate analysis (Reimann et al., 2015)
2) Sensitivity analysis (Pietsch et al., 2008)
3) Heterogeneity of the D_e-distribution (López et al., 2018)

These tracing techniques are relatively new and have to my knowledge not been used in combination with a LEM before. The three techniques are different in spatial and temporal scales (figure 4). Since the techniques are not widely used yet, their performance was first checked on the Allier river terrace samples, with promising results.

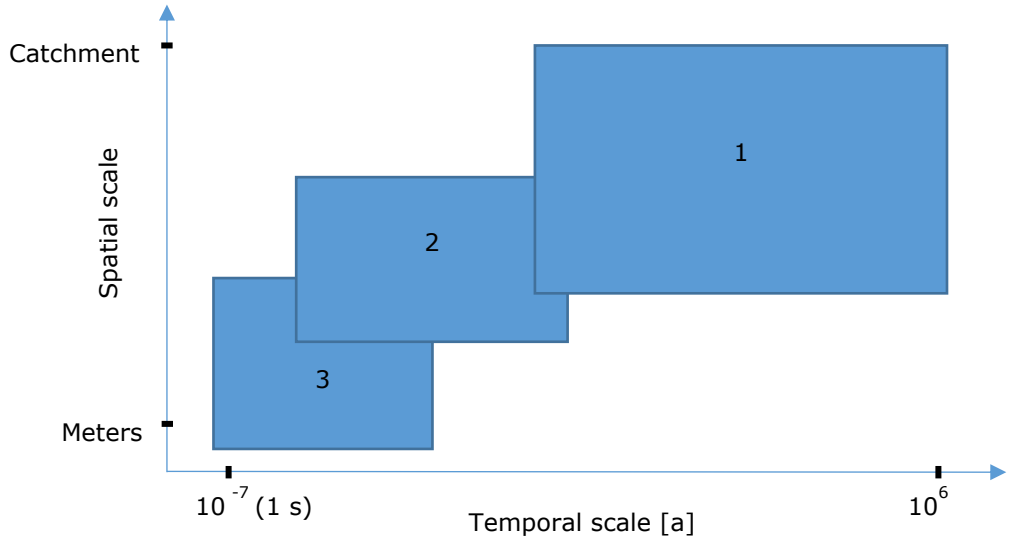

Figure 4. Temporal and spatial scales of the three methods. Size of the boxes does not represent reality. 1. Sensitivity, 2. Bleaching rate, 3. Heterogeneity. LAPSUS (not in this figure) provides information on catchment scale, from one till multiple years.

1.2 Research questions

The main research question is:

When and how did the river landscape of the Allier catchment corresponding to terrace level Fx_{III} evolve?

Previous research showed that quartz grains were non abundant (Broers MSc thesis, 2016), so to improve the chronology I will use single grain (SG) post-IR infrared (pIRIR) feldspar dating. With the SG data I will study the heterogeneity of the sample, the amount of bleaching and the possibility of post-depositional mixing of river sediments, since these subjects are not sufficiently researched yet (Broers MSc thesis, 2016).
I will use the three OSL tracing techniques and LAPSUS to complement the new chronology and to be able to get a clear overview of the river dynamics and river landscape evolution.

The following sub questions will help answering the main question:

1. Is it possible to use the three OSL tracing techniques on the F_{xIII} terrace level of the Allier river?
2. Can we observe differences in fluvial dynamics between the six sampled locations?
3. What information can the LEM LAPSUS provide to this research?
4. How do the method's results (OSL and LEM) compare to each other?
5. What is the age of the Fx_{III} river terrace?

2. Introduction to OSL dating and tracing of river sediments

2.1 Optically Stimulated Luminescence (OSL)

OSL is used for age determination of the burial of quartz and feldspar minerals (Huntley et al., 1985; Preusser et al., 2008). Quartz and Feldspar minerals receive ionizing radiation in the form of alpha, beta, gamma and cosmic radiation, which results in electrons populating electron traps, located between the valence and the conduction band. When particles are stimulated with light or heat, the electrons exit the electron trap and move to a recombination centre and the corresponding energy is released in the form of a luminescence photon. The total resetting of the signal to zero due to exposure to light or heat is called bleaching. The amount of luminescence light stored as trapped charge by quartz and feldspar minerals can be measured in a laboratory and can be related to the time of burial of the particles.

$$Age\ (a) = \frac{Paleodose\ [Gy]}{Dose\ Rate\ [Gy\ a^{-1}]} \quad (1)$$

Equation 1 shows that paleodose and the dose rate are needed for age determination. Paleodose, which is the best estimate of the amount of trapped charge stored during burial, can be reconstructed from a distribution of equivalent dose values (D_e) by comparing the natural luminescence intensity emitted by a sample to the intensity emitted subsequent to a known laboratory dose. The dose rate is the amount of radiation the particles received per year, which can be measured in the laboratory by determining the amount of ^{40}K and using the U/Th decay series (Preusser et al., 2008). OSL can be measured on quartz and feldspar, with possibility to date up until 150 ka and 500 ka, respectively (Wallinga, 2002). Dating is not without assumptions. The dose rate is calculated as an average over time per sample, so for smaller sub samples this dose rate might not be representative. Also anomalous fading and bleaching should be taken into account. Anomalous fading is a thermal loss of charge over time in feldspar minerals (Wintle, 1973; Preusser et al., 2008). Studies show that the amount of anomalous fading can be reduced by using a post-infrared infrared (pIRIR) protocol (Thomsen et al., 2008; Reimann et al., 2012). Fading can also be measured in the laboratory, but Wallinga (2007) shows that these fading rates may underestimate natural fading rates due to preferential trapping.

For correct age determination the grains should be fully bleached before burial, otherwise the age will be overestimated (figure 5). In fluvial environments the chances of incomplete bleaching increase, since the particles are less frequent subject to direct sunlight (Wallinga, 2002). There are several techniques to look whether a sub-sample (aliquot) is incompletely bleached. Usually these incomplete bleached aliquots are not used for age determination because they give overestimated ages, but lately new techniques are developed that are able to use these insufficiently bleached samples. It is thought that it is possible to determine transport rates or transport distances with the amount of bleaching samples received during sediment transport prior to deposition (Reimann et al., 2015; Chamberlain et al., 2017; Bonnet et al., In Review). This we call "tracing", in contrast to "dating" for which OSL normally is used.

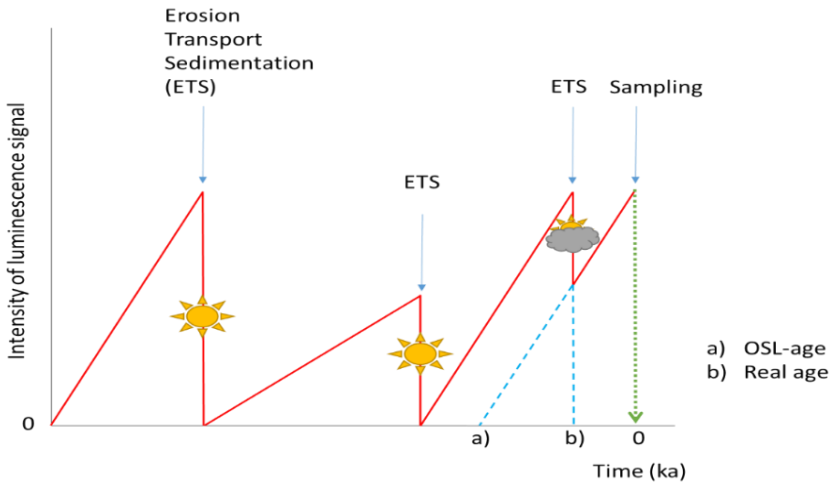

Figure 5. Schematic overview of poor bleaching (after Preusser et al., 2008).

Tracing can be performed in several ways, for example by determining the heterogeneity due to bleaching in equivalent dose distributions. Those distributions contain information about the

transport dynamics in the last cycle of irradiation and burial (Cunningham et al., 2015; López et al., 2018; Bonnet et al., In Review).
A second method is the utilization of the difference in bleaching rates of quartz and feldspar. With this technique it is possible to distinguish different amounts of bleaching, which helps determining the source of the samples and the way of transport (Reimann et al., 2015; Chamberlain et al., 2017). Furthermore, the sensitivity of quartz and feldspar to luminescence can also be measured (Pietsch et al., 2008; Sawakuchi et al., 2011, 2012, 2018). Sensitivity of quartz is thought to increase with each irradiation-bleaching cycle (Pietsch et al., 2008; Sawakuchi et al., 2011, 2012). The higher the sensitivity compared to a source sample, the longer the transport distance of the quartz (Pietsch et al., 2008; Sawakuchi et al., 2011, 2012). Sensitivity is also dependent on the source material (Sawakuchi et al., 2018). This makes it also suitable to determine where a sample originates (sample provenance).

2.2 Bleaching rate analysis

Bleaching rate differs for quartz and feldspar (Chamberlain et al., 2017; Reimann et al., 2015). The bleaching rate of IRSL (infrared stimulated luminescence) and pIRIR (post-infrared IRSL) feldspar signals decreases with increasing measurement temperatures (Reimann et al., 2015). Because the rate differs, it is possible to compare the different rates in one sample, to determine the bleaching in all components. It is thought that it would be possible to gain information about transport dynamics through the differences in bleaching (Reimann et al., 2015). This method provides information on the last bleaching cycle of quartz and slow-bleaching feldspar. Therefore this method will give results over short to intermediate spatial and temporal scales (figure 4).
Previous research used the different bleaching rates to assess the amount of bleaching in a sample. Reimann et al. (2015) determined the age of beach samples with blue light OSL on quartz (BSL), at different measurement temperatures for feldspar, and the very slow bleaching thermoluminescence (TL). Since quartz bleaches very fast, this will be the most certain age. A ratio with the BSL age is calculated for the slower bleaching IRSL and pIRIR measurements. The form of the resulting graph then tells how well a sample is bleached (figure 6). Chamberlain et al. (2017) used the same technique, but they normalized to the BSL equivalent dose, since their samples did not have a common primary depositional age (equation 2).

$$BI_{LS} = \frac{D_{eBSL}(D_{eLS}-D_{eBSL})}{D_{eBSL}+1} \qquad (2)$$

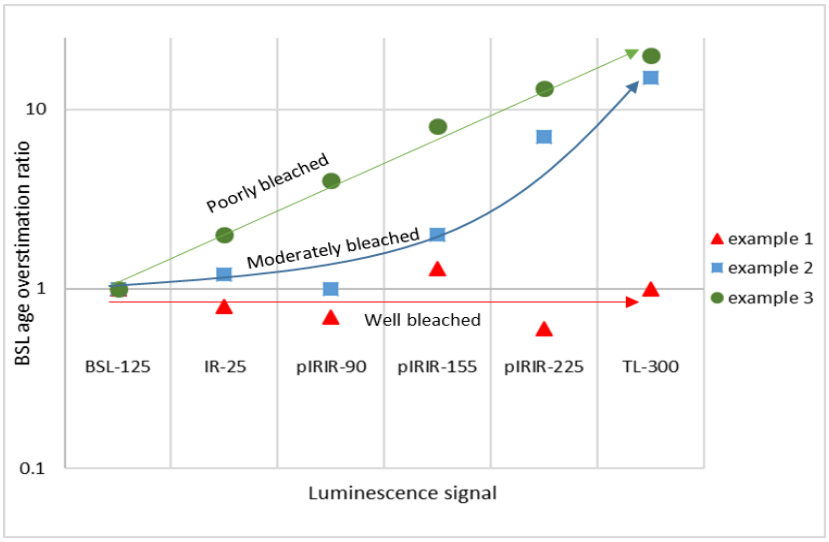

Figure 6. Example of BSL age overestimation ratio. Numbers in this graph are fictional (After Reimann et al., 2015).

2.3 Sensitivity analysis

Pietsch et al. (2008) describe sensitivity as the "efficiency with which the radiation dose is expressed as emitted photons during the measurement process". As already stated before, the sensitivity is thought to increase with each irradiation-bleaching cycle (Pietsch et al., 2008; Sawakuchi et al., 2011, 2012). Therefore this method can be used to determine the source of the grains and the total transportation distance. This method provides thus information on the largest temporal and spatial scales (figure 4).

First experiments have been conducted using quartz sensitivity. For example, Pietsch et al. (2008) determined the sensitivity of quartz in an ephemeral river in Australia. They discovered that sensitivity increases downstream. They simulated the irradiation-bleaching cycles in the laboratory and found that this indeed increases the sensitivity of the quartz grains. The more sensitive a quartz grain is, the more erosion-transportation-deposition cycles it experienced, the larger the transport distance probably is. Sawakuchi et al. (2011, 2012, 2018) did multiple studies on sensitivity of quartz in Brazil (e.g. Amazonas basin). They found that the sensitivity is not only dependent on the burial cycles, but also on the source material. They also found that sensitivity and denudation rate are linearly correlated, so sensitivity can be a proxy for erosion as well. Feldspar sensitivity is not yet investigated.

2.4 Heterogeneity of D_e distribution

Heterogeneity is the distribution of the equivalent doses per sample. This method is normally used on quartz minerals (Bailey & Arnold, 2006; Cunningham et al., 2015; López et al., 2018). Feldspar heterogeneity has not been studied extensively, but might prove interesting as well.
This method will provide information on the shortest temporal and spatial scales (figure 4).
For well bleached samples, the log-normal D_e distribution will look Gaussian, while for poorly bleached samples this distribution will look skewed (Bailey & Arnold, 2006). There are several ways for describing the heterogeneity of such distributions. Cunningham et al. (2015) developed a so called poor-bleaching score, and López et al. (2018) used over-dispersion (OD), which is a quantitative measure of the scatter of the dose distribution. López et al. (2018) used OD as a proxy for sedimentary chaos to determine whether sedimentary layers were deposited by storms or tsunamis. A higher OD, so more partially bleached grains, means a high-energy way of transport, because there is less light due to turbidity or a high sand density.

3. Methods

Figure 7 below shows a summary of the approach used in this research.

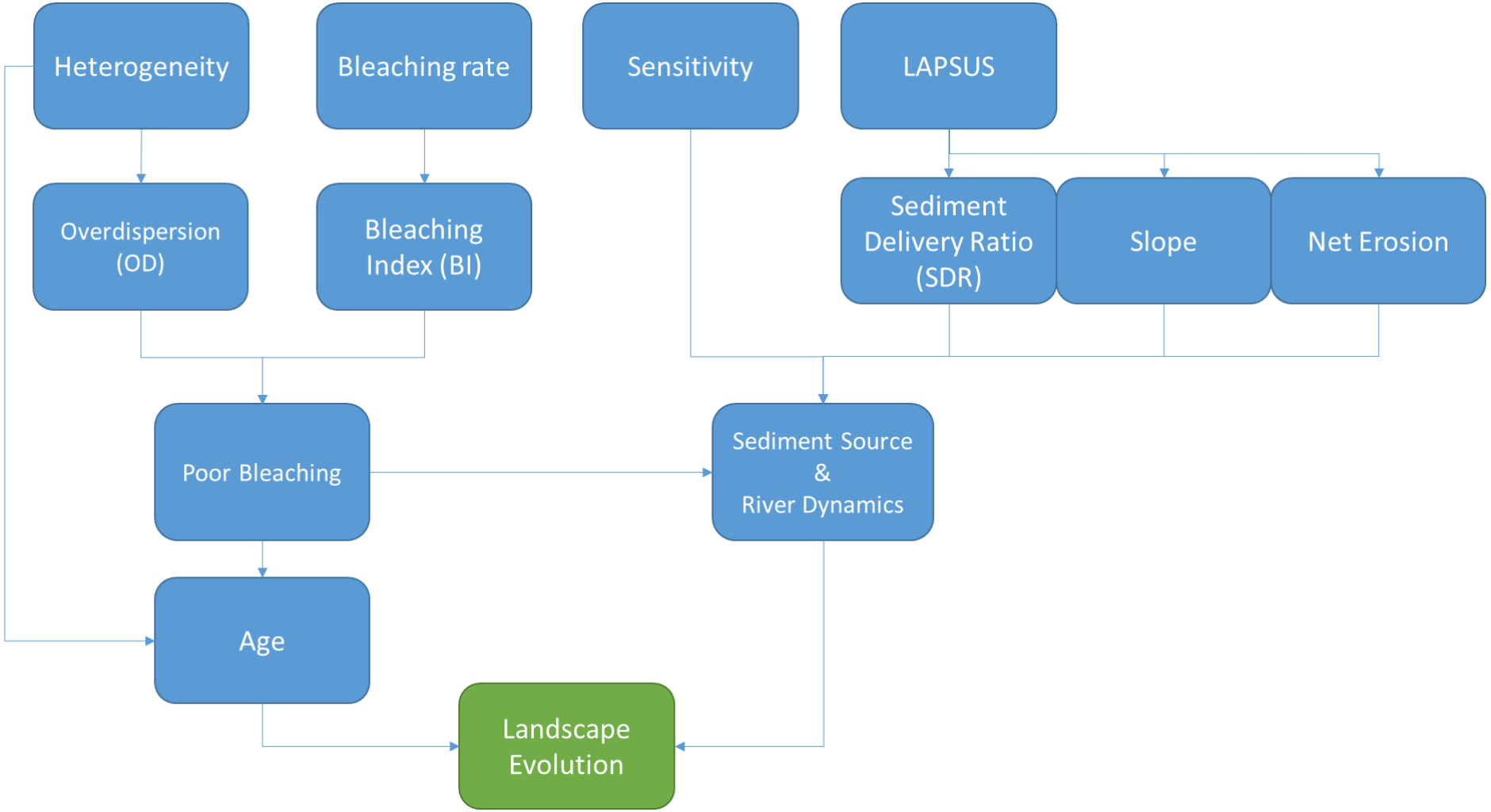

Figure 7. Flow chart of approach used in this research.

3.1 Experimental details

The six samples used for this research were already taken by Broers (2016). The correct order of the samples is shown in table 1, with sample -177 closest to the source and -187 furthest. In figure 8 the sampling locations are shown.

Table 1. Correct sample order from upstream to downstream of the Allier river.

Sample Code: NCL-2515 ###	Distance to source (km)	Coordinates	
		UTM 31T	UTM O
177	176.4	516953	5067324
182	181.9	520445	5074042
180	190.1	525162	5078400
190	205.8	536103	5088600
188	215.8	537433	5097093
187	216.5	536692	5097786

The OSL measurements were done using an automated Risø TL/OSL reader at the Netherlands Centre for Luminescence. The heterogeneity and sensitivity experiment were both done using single grain (SG) measurements for quartz and feldspar (López et al., 2018; Pietsch et al., 2008). The bleaching rate experiment was done on polymineral samples (Chamberlain et al., 2017; Reimann et al., 2015).

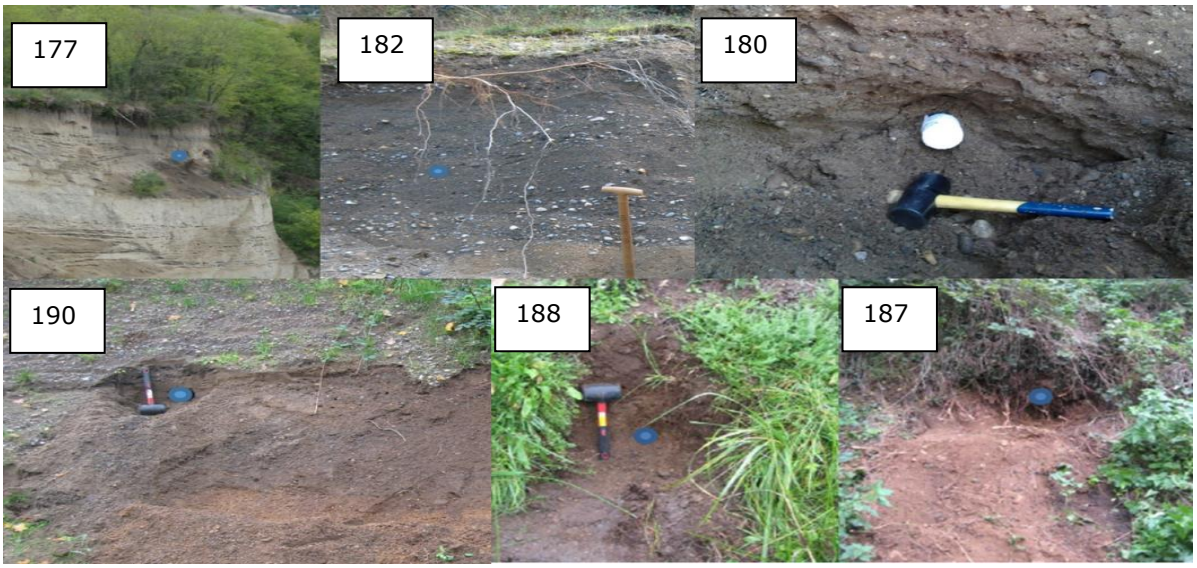

Figure 8. Sampling locations (Broers, 2016).

3.1.1 Polymineral measurements

The polymineral samples were not pre-treated yet by Broers (2016). The samples were sieved to retrieve a grain size fraction of 250-300 µm and received a pre-treatment of 40 minutes of HCl and 30 minutes of H_2O_2 to remove carbonates and organic material. After this the aliquots were prepared with an 8 mm mask.

The following measurements were done in this experiment: Quartz 125°C, IRSL-25, pIRIR-90, pIRIR-155, pIRIR-225 and TL (after Chamberlain et al., 2017; Reimann et al., 2015). The polymineral samples were measured with interchangeable filters. For quartz a U-340 filter (7.5 mm) and for feldspar a blue filter package was used. The samples were irradiated with a $^{90}Sr/^{90}Y$ beta-source providing a dose rate of 0.0821 ± 0.003 Gy/s.

The measurement protocol for this experiment, the so-called MS-SAR approach, is shown in table 2.

Table 2. MS-SAR protocol for the polymineral measurement.

Step	PMS-SAR protocol
1	Natural/Regenerative Dose*
2	Preheat of 250°C for 10.0s (5.00°C/s)
3	IR LED at 50°C for 108.0s (2.00°C/s)
4	IR LED at 90°C for 108.0s (2.00°C/s)
5	IR LED at 155°C for 108.0s (2.00°C/s)
6	IR LED at 225°C for 500.0s (2.00°C/s)
7	Blue light OSL at 125°C for 20.0s (2.00°C/s)
8	Test dose (8 Gy)
9	Preheat of 250°C for 10.0s (5.00°C/s)
10	IR LED at 50°C for 108.0s (2.00°C/s)
11	IR LED at 90°C for 108.0s (2.00°C/s)
12	IR LED at 155°C for 108.0s (2.00°C/s)
13	IR LED at 225°C for 108.0s (2.00°C/s)
14	Blue light OSL at 125°C for 20.0s (2.00°C/s)
15	TL up to 300°C
	Repeat from step 1
	*Irradiation in the following order: Natural - 20Gy - 40Gy - 96Gy - 0Gy - 20Gy

3.1.2 Single grain measurements

The grain size fraction used to fill the SG-aliquots was 212-250 µm. The quartz and feldspar of this fraction were already pre-treated by Broers (2016). For quartz measurements a U-340 filter was used, for feldspar measurements an I-410 filter. The samples were irradiated with a $^{90}Sr/^{90}Y$ beta-source providing a dose rate of 0.1002 ± 0.004 Gy/s.
The quartz was measured once (green light OSL), while feldspar was measured thrice: IRSL-50, pIRIR-150 and pIRIR-225. The measurement protocols are shown in table 3.
These measurements are used for the sensitivity analysis, the heterogeneity of D_e-distribution and for age determination. For age determination dose recovery and fading tests are required, to measure residual dose and fading rate respectively. The explanation of the measurements for these tests can be found in appendix A2.

Table 3. Measurement protocols for Single Grain measurements. Left: Feldspar measurement. Right: Quartz measurement.

Step	Feldspar SG protocol
1	Natural/Regenerative Dose*
2	Preheat of 250°C for 120.0s (5.00°C/s)
3	SG IRSL at 50°C for 2.0s
4	SG IRSL at 150°C for 2.0s
5	SG IRSL at 225°C for 2.0s
6	IR LED at 225°C for 500.0s (5.00°C/s)
7	Test dose (10 Gy)
8	Preheat of 250°C for 120.0s (5.00°C/s)
9	SG IRSL at 50°C for 2.0s
10	SG IRSL at 150°C for 2.0s
11	SG IRSL at 225°C for 2.0s
12	IR LED at 225°C for 500.0s (5.00°C/s)
	Repeat from step 1
	*Irradiation in the following order: Natural - 10Gy - 20Gy - 40Gy - 80Gy - 160Gy - 0Gy - 10Gy

Step	Quartz SG protocol
1	Natural/Regenerative Dose*
2	Preheat of 260°C for 10.0s (5.00°C/s)
3	IR LED at 50°C for 100.0s (2.00°C/s)
4	SG Green light OSL, 125°C for 1.0s
5	Test dose (10 Gy)
6	Preheat of 240°C for 10.0s (5.00°C/s)
7	IR LED at 50°C for 100.0s (2.00°C/s)
8	SG Green light OSL at 125°C for 1.0s
9	Blue light OSL at 270°C for 40.0s (2.00°C/s)
	Repeat from step 1
	*Irradiation in the following order: Natural - 10Gy - 20Gy - 40Gy - 0Gy - 10Gy

3.1.3 LAPSUS

LAPSUS uses a DEM to calculate erosion and sedimentation for a catchment (Schoorl et al., 2000). A digital elevation model (DEM) of 25x25m was used (figure 9), which was the smallest grid size that could be used to run the whole Allier catchment in LAPSUS. Smaller grid sizes resulted in too large data files that could not be used by LAPSUS.

In LAPSUS the sedimentation and erosion rate were determined for low and high rainfall intensity (250 and 800 mmy^{-1}). Other parameters such as sedimentation, soil depth and erodibility were set to default values for simplicity reasons.

With the resulting first and second order DEM derivatives, and third order erosion and sedimentation maps (figure 10) the following variables were calculated in ArcGIS (version 10.4.1): Flow accumulation, slope, net erosion and sediment delivery ratio for low as well as high rainfall intensity. The flow accumulation tool in ArcGIS (Jenson & Domingue, 1988; Tarboton et al., 1991) calculates accumulated flow based on a slope map where all sinks have been removed. The slope map is a raster dataset, providing a direction in which the water will flow per cell. The flow accumulation tool sums all cells flowing into each downslope cell in the output raster (Jenson & Domingue, 1988). The resulting map shows all the places in the catchment where water accumulates, i.e. creeks and rivers. Since all sinks are removed from the DEM, all cells flow eventually towards the catchment outlet, which thus has the highest flow accumulation value.

To get a better grip on the sediment delivery the Allier catchment was divided into sub-catchments, following the protocol by Parmenter & Melcher (2012) (figure 11). The absolute (net) erosion per sub catchment is calculated by subtracting the absolute value of total sedimentation of the absolute value of total erosion within the sub catchment (equation 3).

$$Erosion = |Total\ Erosion| - |Total\ Sedimentation| \quad (3)$$

The sediment delivery ratio shows the balance between total erosion and total sedimentation for an area, in this case the sub catchments. Originally the SDR is calculated as the sediment yield divided over the total erosion in an area (Lu, Moran, & Prosser, 2006). LAPSUS does not calculate sediment yield, but total sedimentation. Therefore SDR is calculated with equation 4:

$$SDR = 1 - \left(\frac{|Total\ Sedimentation|}{|Total\ Erosion|}\right) \quad (4)$$

The SDR values range between zero and one. SDR = 1 means there is no sedimentation, i.e. all eroded sediments leave the sub catchment. SDR = 0 means the opposite, i.e. all eroded sediments are deposited within the sub catchment.

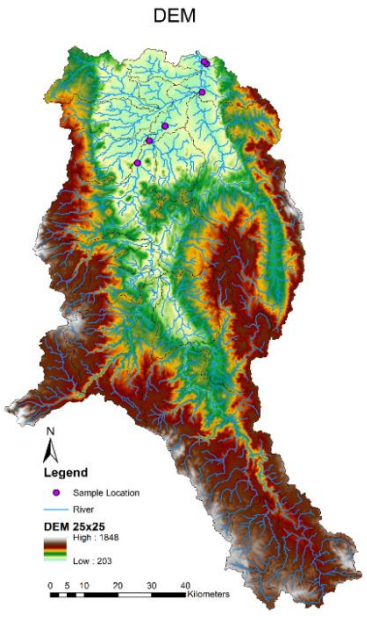

Figure 9. DEM of the Allier catchment.

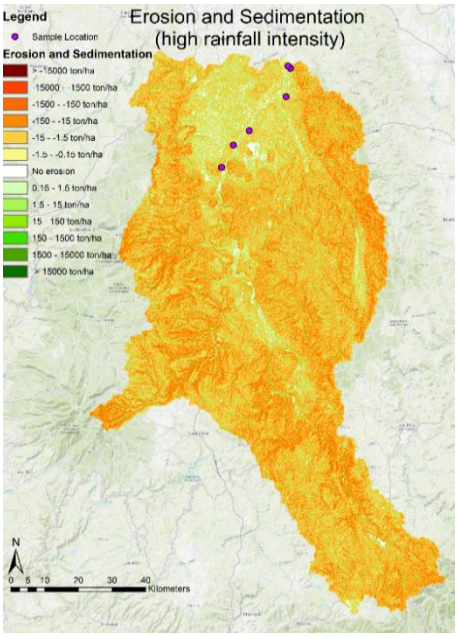

Figure 10. Erosion and sedimentation map of the high rainfall intensity scenario. The low rainfall scenario shows the same patterns, but with less amounts of erosion and sedimentation.

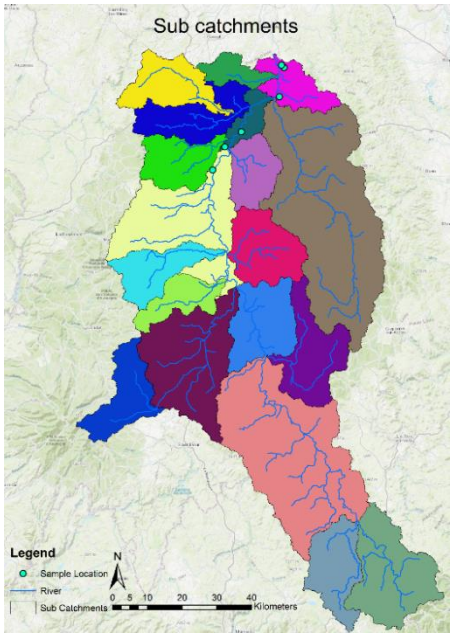

Figure 11. Sub catchments of the Allier catchment.

3.2 Analysis

3.2.1 Bleaching Rate Analsysis

The data gained from the Risø Analyst (version 4.31.9 (Duller, 2015)) was accepted with the conditions shown in table 4. This was done for all measurements except for the TL measurement and quartz, since the TL measurement has no test dose and recuperation point and quartz did not yield any results.

All accepted data were further processed in R, where the luminescence package (Kreutzer et al., 2018) provided the Central Age Model (CAM) and Minimum Age Model (MAM) equivalent doses (Burow, 2018a, 2018c). To calculate the D_e for the TL-measurements, the natural dose was interpolated between the nearest equivalent dose points, since a trend line forced through zero was not possible for these points (figure 12). This makes the calculation of the D_e inaccurate. Since there is no test dose available for TL, no error can be calculated.

With the D_e-values per measurement the bleaching index (BI) can be calculated. Equation 2 is used to calculate this index, where subscript LS stands for the luminescence signal of choice and BSL is the luminescence of the quartz measurement (Chamberlain et al., 2017).

$$BI_{LS} = \frac{D_{eBSL}(D_{eLS}-D_{eBSL})}{D_{eBSL}+1} \qquad (2)$$

Unfortunately the quartz did not provide luminescence signals. Instead of the BSL measurement, the IRSL-25 measurement, as the fastest bleaching measurement next to quartz, is used to normalize the other measurements.

Table 4. Accepting condition PMS-SAR. OSL-signal and Background signal indicate the integrals over which this signal is measured (depending on time of measurement).

Accepting conditions PMS-SAR	
Max. measurement error (%)	2.5
Monte Carlo repeats	1000
Recycling ratio limit (%)	20
Max. test dose error (%)	20
OSL-signal (s)	
IR-25/90/150	4.4-4.8
IR-225	20.4-22.2
Background signal (s)	
IR-25/90/150	16-20
IR-225	74.1-92.6

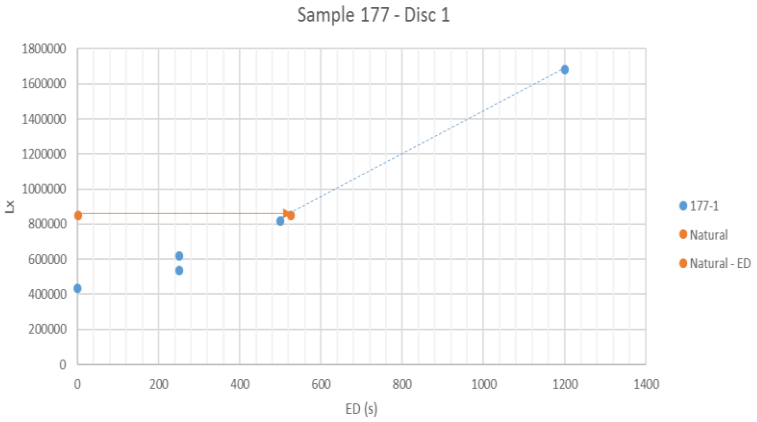

Figure 12. Example of TL-D_e determination. Blue dots: regenerative dose points. Orange: Natural signal.

3.2.2 Sensitivity Analysis

The OSL sensitivity of the grains was obtained by taking the OSL and background integral of the Linear Modulated OSL curves (table 5, Sawakuchi et al., 2011). When the OSL minus the background signal was above a threshold (45 for quartz and 100 for feldspar), they were accepted for further analysis. The sensitivity in percentages is the amount of accepted sensitive grains per sample divided over the total amount of grains on the SG-discs.

Table 5. Accepting conditions SG measurements. OSL-signal and Background signal indicate the integrals over which this signal is measured.

Accepting conditions SG	Q	FS
Max. measurement error (%)	2.5	2.5
Monte Carlo repeats	1000	1000
Recycling ratio limit (%)	30	20
Max. test dose error (%)	30	20
OSL-signal (s)	0.100-0.133	0.200-0.267
Background (s)	0.667-0.833	1.33-1.67

3.2.3 Heterogeneity of D_e-distribution

For this technique the analyst programme of Risø was used (version 4.31.9 (Duller, 2015)). The Risø analyst programme accepted or rejected grains based on the conditions shown in table 5.
The resulting amount of accepted grains displayed high and low outliers. These were removed by iterating the dataset per sample over the (iterated) sample mean (μ) ± 2σ.
With the resulting dataset the over-dispersion (OD) could be calculated in R (Burow, 2018a) and KDE and Radial plots could be produced (appendix A3) (Dietze & Kreutzer, 2018a, 2018b).
From this the heterogeneity could be determined for each measurement temperature (50, 150, 225 °C respectively, see table 2) and quartz (where possible).

3.2.4 Dating of river terrace Fx_{III}

The dataset of the heterogeneity analysis was also used for age determination. CAM and MAM were calculated in R, using a σ_b value of 0.15 for the MAM (see chapter 4.4 for justification). Quartz did not provide useable data, so further analysis was done on feldspar measurements. In sample 187 low dose populations were observed, so a Finite Mixture Model (FMM) (Burow, 2018b) was applied to uncover how many dose populations were present in the sample. The FMM, for which also a σ_b of 0.15 was used, showed that six different dose populations could be found within this sample. The oldest two populations are used to determine the D_e, because the oldest samples are hardest to preserve, while younger samples can be mixed in due to for example bioturbation.

Furthermore a dose recovery test and fading analysis were performed. The dose recovery test showed that all measurement temperatures had a residual dose, increasing per measurement temperature (table 6). Fading analysis in R (Kreutzer, 2018) according to the Huntley & Lamothe (2001) correction model revealed that only the 50°C-measurement needed a fading correction of 9.09 ± 2.04 %/decade. The 150°C and 225°C measurement did not show anomalous fading.

Table 6. Residual doses per measurement.

Residual Dose (Gy)	
50°C	-1.56 ± 0.57
150°C	-2.951 ± 0.71
225°C	-6.033 ± 1.562

From the three measurement temperatures for feldspar, the pIRIR-150 measurement has least amount of luminescent grains. The measurements at this temperature are therefore omitted from further analysis.

4. Results

4.1 Bleaching Rate Analysis

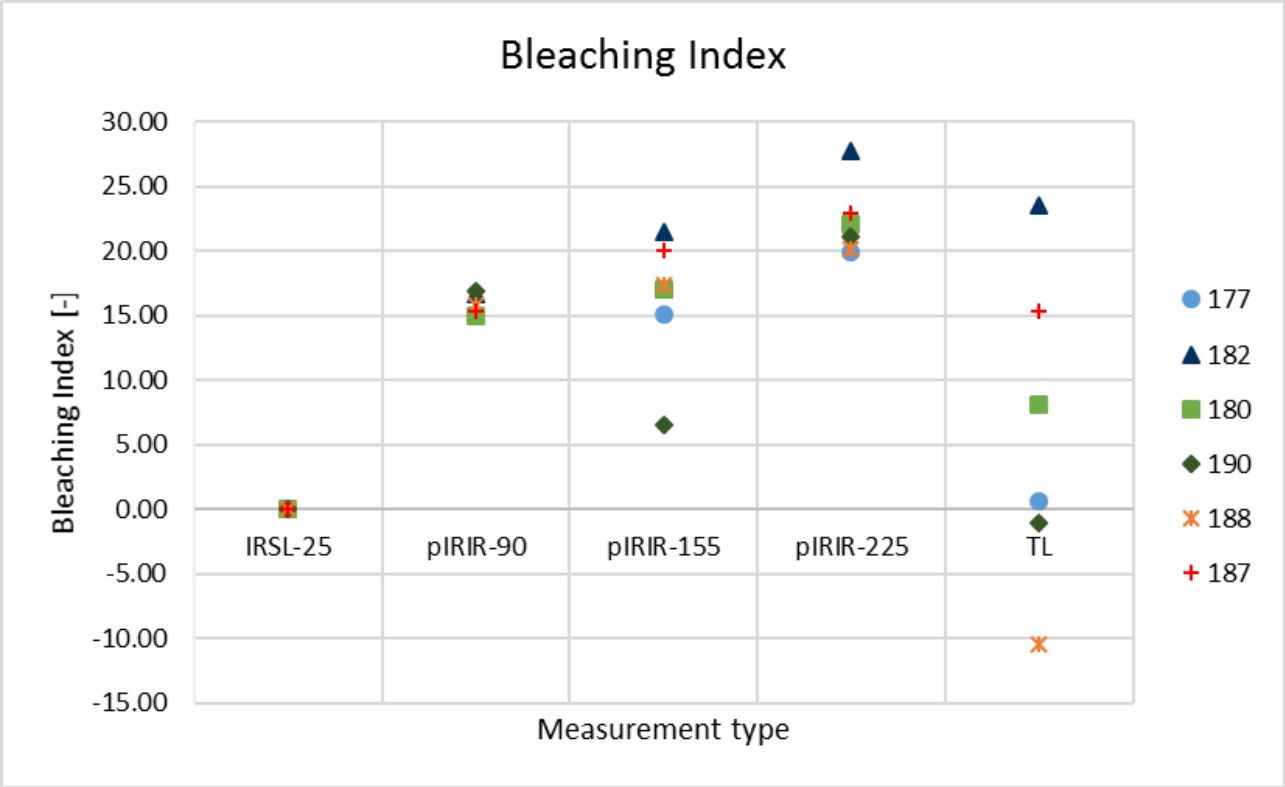

Figure 13. Bleaching Index [-]. Samples in legend from upstream to downstream.

Figure 13 shows the bleaching index (BI). The spread per measurement is small, except for the inaccurately calculated TL measurement. pIRIR-155 shows the highest variation between samples. Sample 182 shows highest BI in almost all measurements, so this sample would be poorest bleached. Despite this, the samples all show similar inter sample trends, meaning they show similar amounts of bleaching.

As already mentioned, quartz was not luminescent in this measurement although quartz grains can be seen on the discs (appendix A4). Furthermore, the discs show a variety of other minerals than feldspar and quartz. This variety in mineralogy could have been diminished when using density separators to separate the heavy minerals.

Since the quartz could not be used for the normalisation of the bleaching index, the lowest temperature feldspar measurement was taken (IRSL-25). This measurement has the fastest bleaching component and is therefore most likely best bleached, but it suffers from anomalous fading, introducing an undesired uncertainty into the analyses. The BI is very dependent on the values used for normalisation, so it is arguable whether BI based on IRSL-25 normalisation are meaningful. However, inter sample trends in the BI can be still visible, even with an unstable normalising factor, so the BI can still be used to compare the relative amount of bleaching among the six samples.

The TL is only measured once per regeneration (table 2), so there is no test dose available. This makes the measurement unreliable and no error calculation was possible. The calculation of the equivalent dose also was imprecise. Figure 12 shows that the regenerative dose points don't go through zero, which makes the use of a trend line through all points impossible. Interpolation between the nearest dose points was therefore necessary for calculating the TL-D_e, which makes the other dose points useless for the TL calculation.

4.2 Sensitivity Analysis

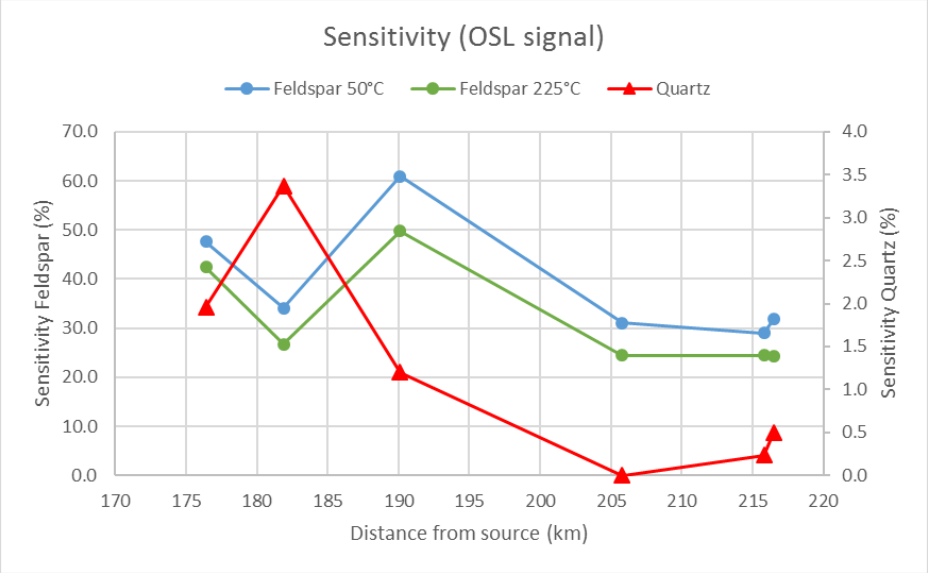

Figure 14. Sensitivity of feldspar (left y-axis) and quartz (right y-axis) grains. Samples are displayed from upstream to downstream (-177, -182, -180, -190, -188, -187).

Figure 14 shows that the quartz (right y-axis) provided far less signals compared to feldspar (left y-axis) measurements. Quartz is far less sensitive compared to feldspar samples: 0.0-3.5% vs. 25-63% for quartz and feldspar, respectively (figure 14).
There seems to be a general decline in quartz sensitivity downstream the Allier river. One of the quartz samples (-190) showed serious feldspar contamination, which can be taken as prove that the quartz was not luminescent at all, or that the feldspar overshadowed this little amount of quartz signal. A magnetic separator should have been used to remove (most of) the feldspar in the quartz samples (Porat, 2006).
What is striking in figure 14, is that the quartz and feldspar sensitivity looks to be opposite of each other for the first three samples. Where feldspar sensitivity drops, quartz sensitivity increases and vice versa. The last three samples did not have any sensitive quartz (only one grain produced luminescence on ± 400 measured grains) and feldspar seems to be on a certain base level, meaning there is no trend with distance from source. The drop in quartz sensitivity could mean that the quartz in the last three samples experienced less burial-irradiation cycles (i.e. shorter transportation, (Pietsch et al., 2008)) or the quartz originates from a different source area (Sawakuchi et al., 2018).

4.3 Heterogeneity

Originally this experiment was meant to be done on quartz and feldspar minerals, but due to little available quartz in the samples, only feldspar has been used to carry out this experiment.
Figure 15 shows the over-dispersion (OD) of the six samples from two measurement temperatures (IRSL-50 & pIRIR-225). OD can be explained as the scatter of the dose distribution that does not originate from instrumental noise (López et al., 2018). A high OD thus represents a more heterogeneous bleached sample. The over-dispersion shown in figure 15 indicates a low variability between the samples and between the measurements. Almost all measurements have an OD of <20%. Only sample 190 till sample 187 (the three downstream samples) show significant differences between the measurement temperatures. This can be caused by heterogeneous bleaching and/or by mixing e.g. due to bioturbation. When looking at the radial plot and KDE plot of sample 187 (figure 15) multiple populations can be seen within the sample, with very young signals of less than 1 Gy to older signals up to 60 Gy. Because the sample was taken into a soil horizon (figure 8) and the age tends to be much younger than for the other samples due to the younger populations in the distribution, it is thought that the high heterogeneity stems from bioturbation.

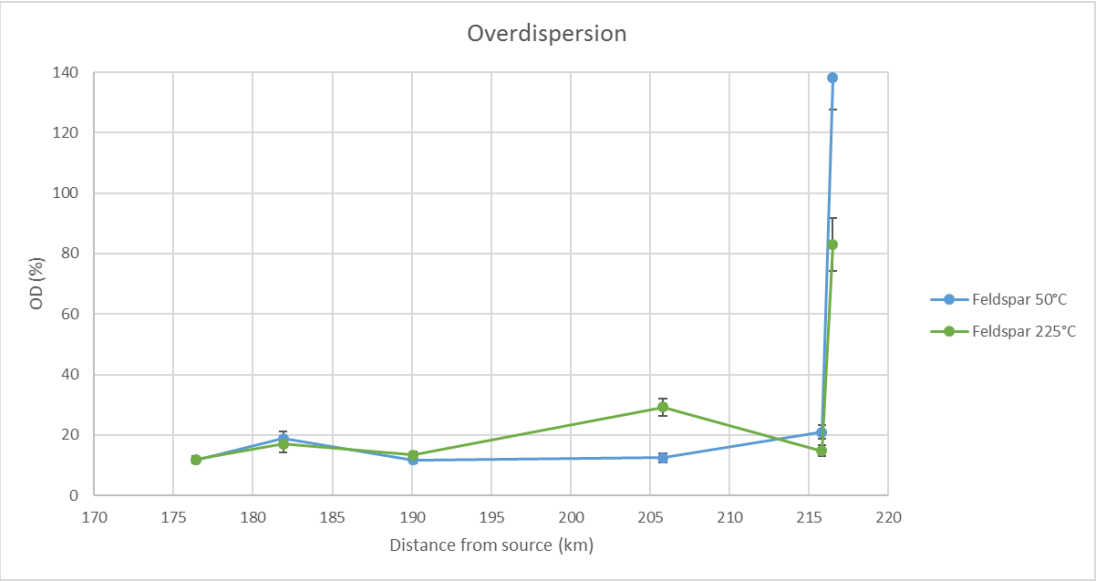

Figure 15. Over-dispersion for two SG feldspar measurements (IRSL-50 and pIRIR-225), including errors. Samples are displayed from upstream to downstream (-177, -182, -180, -190, -188, -187).

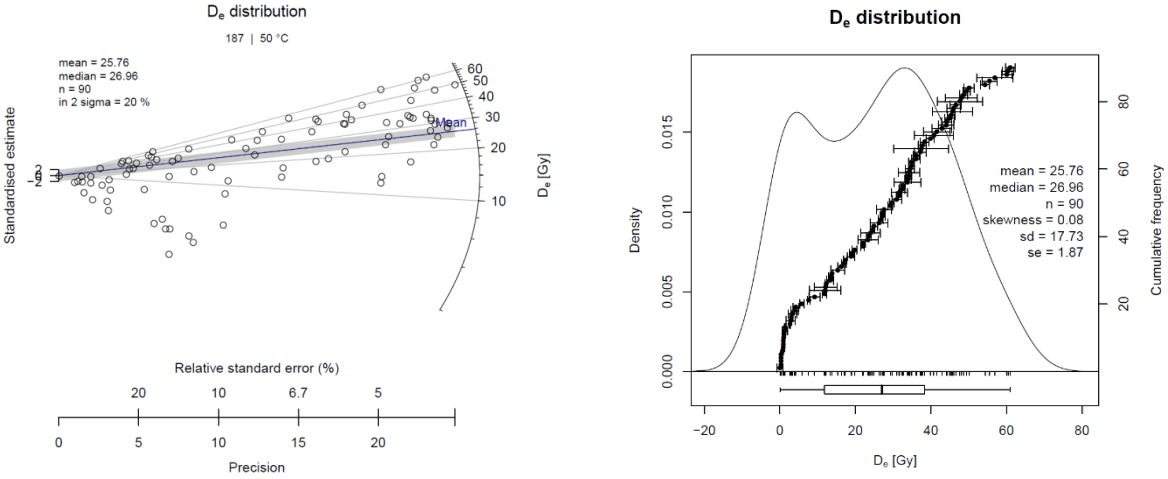

Figure 16. Radial plot (left) and KDE plot (right) of sample 187, IRSL-50 measurement. Multiple populations can be seen in both plots. The radial plots of the other samples can be seen in appendix A3.

4.4 Dating of river terrace Fx_{III}

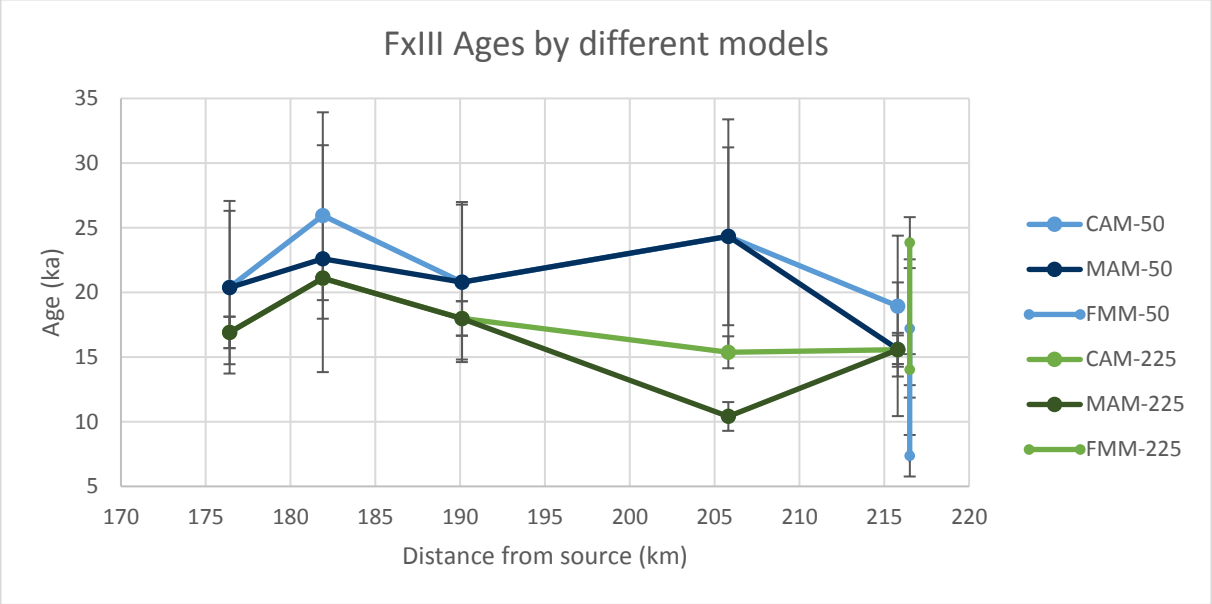

Figure 17. Ages with corresponding errors calculated with different measurement temperatures and age models. CAM = Central Age Model, MAM = Minimum Age Model, FMM = Finite Mixture Model (only for sample 187). All ages are fading corrected. Samples are displayed from upstream to downstream (-177, -182, -180, -190, -188, -187).

Figure 17 shows the ages after fading and residual dose correction for the IRSL-50 and pIRIR-225 measurement, including the FMM-age range for sample 187.
The CAM as well as the MAM age are incorporated in figure 17. For the MAM (as well as for the FMM) a value for σ_b had to be chosen. There were several options:

- 0.2 (default in R)
- 0.21 (lowest OD in original dataset)
- 0.27 (average OD in iterated dataset)
- 0.15 (average OD of IRSL-50 sample 177-188, iterated dataset)

Since the data I used was from the iterated dataset, the first two options already are out of question. The differences in MAM using 0.27 and 0.15 were negligible. Because sample 187 has a very high OD due to bioturbation, I decided to not take this value into account for the σ_b value. This results in the value of 0.15 being chosen to calculate the MAM. When the OD of a sample is around or below 15%, the MAM and the CAM are then the same.

For the CAM-225 calculation, sample 182 is older than the other samples. The OD of this sample is comparable to the other samples, but the Bleaching index is highest for this sample. This could mean that the sample is not heterogeneously poor bleached, but homogeneously poor bleached. This means that it is possible that this sample shows an offset in age (figure 18) and thus that the burial of this sample occurred later than the data suggests.

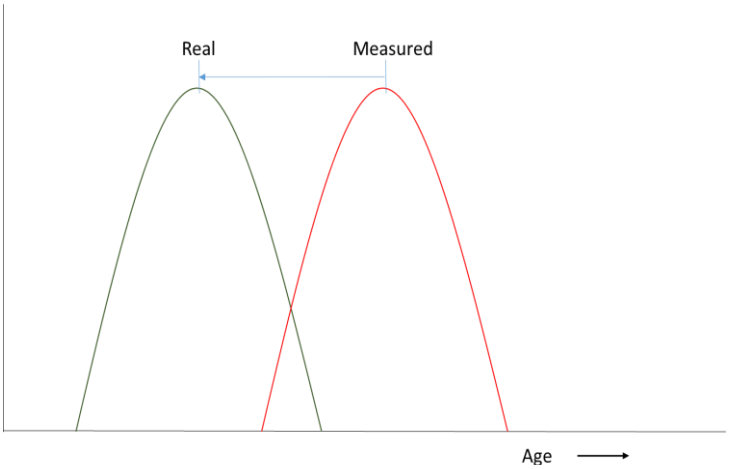

Figure 18. Schematic visualisation of age offset due to homogeneous incomplete bleaching.

Age decision
To come to the age of this river terrace, a decision has to be made between several measurement temperatures and models.

- MAM vs. CAM

The MAM and CAM are almost the same, due to the low OD values and the chosen σ_b. Usually MAM is chosen when samples are heterogeneous poorly bleached. The BI and OD show that this is not the case for this terrace, so the MAM is not needed. The CAM ages will be used in further analysis.

- IRSL-50 vs. pIRIR-225

The IRSL-50 measurement fades, with an unusual high g-value of 9.09 ± 2.04 %/decade. Normal g-values range between 3-5%/decade (Reimann et al., 2011). This increases the error of the age with approximately 5 ka. The pIRIR-225 measurement does not fade. However, this measurement has higher risk of incomplete bleaching, which could result in increased ages. In figure 13 can be seen that the BI is highest for the pIRIR-225 measurement, indicating that the samples are poorest bleached at this measurement temperature. Sample 182 shows the highest BI of all samples, but apart from that the relative amount of poor bleaching is comparable. This leads to the conclusion that while the pIRIR-225 measurement might be poorest bleached, it at least is roughly the same for all samples. Therefore the pIRIR-225 measurement is chosen for further analysis.

The resulting age for the terrace can be seen in figure 19 and table 7. The age range of sample 187 will not be included in further analysis in the following chapters, because the range shows that it is impossible to come up with one age for this sample. To avoid wrong conclusions about the terrace because of this range, it is therefore omitted.

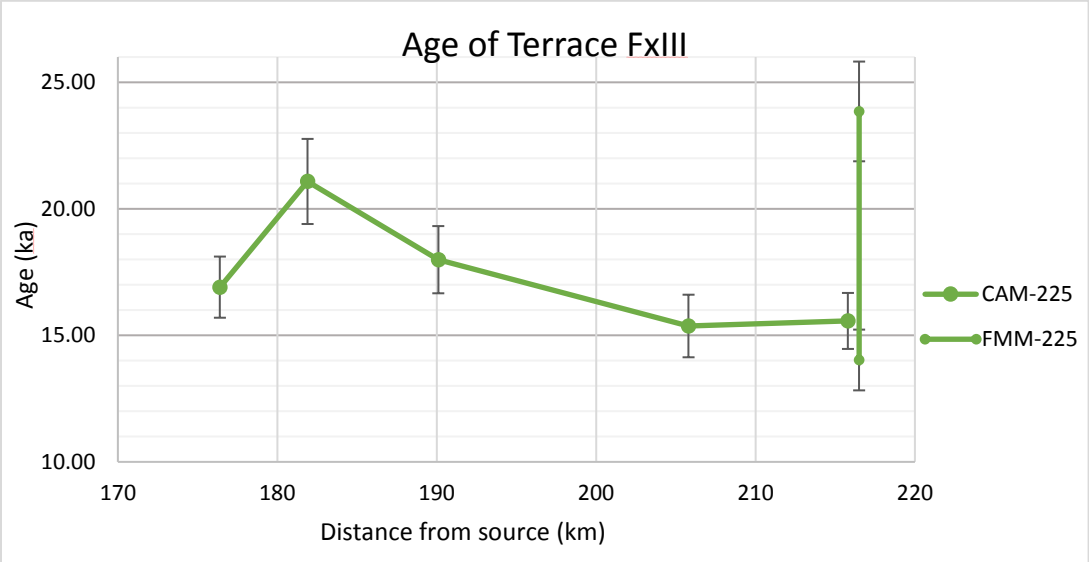

Figure 19. Resulting age for terrace level Fx_{III} (fading corrected). Samples are displayed from upstream to downstream (-177, -182, -180, -190, -188, -187).

Table 7. Fading corrected ages of Fx_{III} terrace samples.

Age per sample (ka)	
177	16.91 ± 1.21
182	21.08 ± 1.68
180	17.99 ± 1.33
190	15.37 ± 1.24
188	15.57 ± 1.11
187	14.03 ± 1.20 – 23.85 ± 1.97

4.5 LAPSUS

The slope map (figure 20) shows that the northern part of the catchment has less steep slopes than the southern upstream part of the catchment. The eastern rift shoulder is nicely visible in the map, just as the valley of the Allier river and the Dore tributary. In the south-western part of the catchment steeper slopes can be found.
The Sediment Delivery Ratio maps (figure 21 and 22) show that SDR is almost always above 0.5, indicating that all sub catchments erode more than that they deposit in the catchment. The southern (upstream) catchments have the highest SDR, a few catchments in the north have the lowest SDR.
Figure 23 and 24 show net erosion. It can be seen that two sub catchments provide the highest amount of eroded material. These catchments have both a high SDR (above 0.75), indicating that both catchments have more erosion compared to sedimentation, but the ratio for both catchments is the same. Larger sub catchments present higher values here, since this parameter is dependent on the area. The two catchments with highest net erosion are the two largest catchments (>1000 km^2).

The LAPSUS model was not calibrated for this area and for instance the erodibility was set to a default value. Unfortunately no detailed geological map is available for this area, but figure 1 shows that the area contains several different lithological units with different erodibility, from Oligocene sandstone to basalts and granites. Therefore the maps shown below only give a rough indication of the sedimentation and erosion in the Allier catchment.

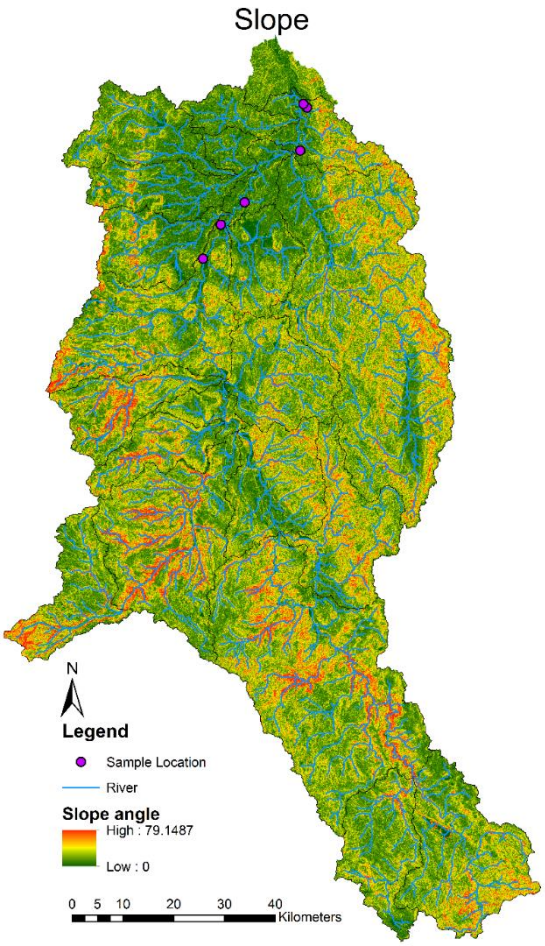

Figure 20. Slope in degrees.

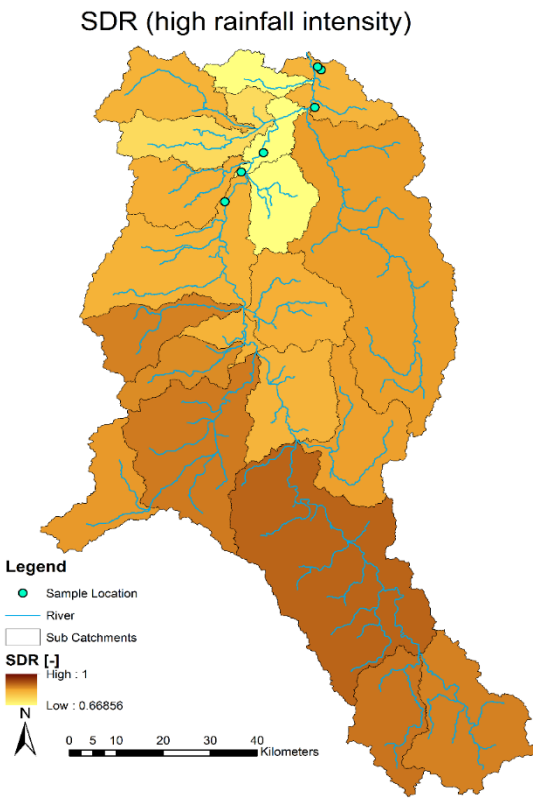

Figure 21. Sediment Delivery Ratio per sub catchment for the high rainfall intensity scenario.

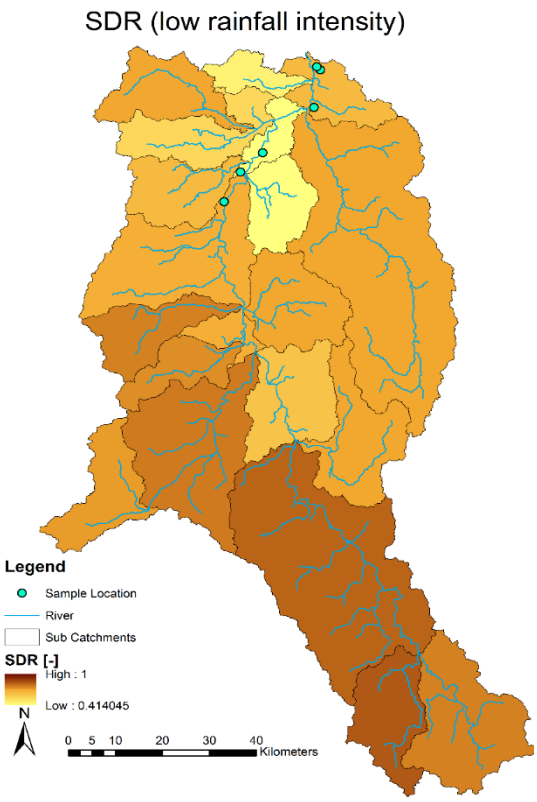

Figure 22. Sediment Delivery Ratio per sub catchment for the low rainfall intensity scenario.

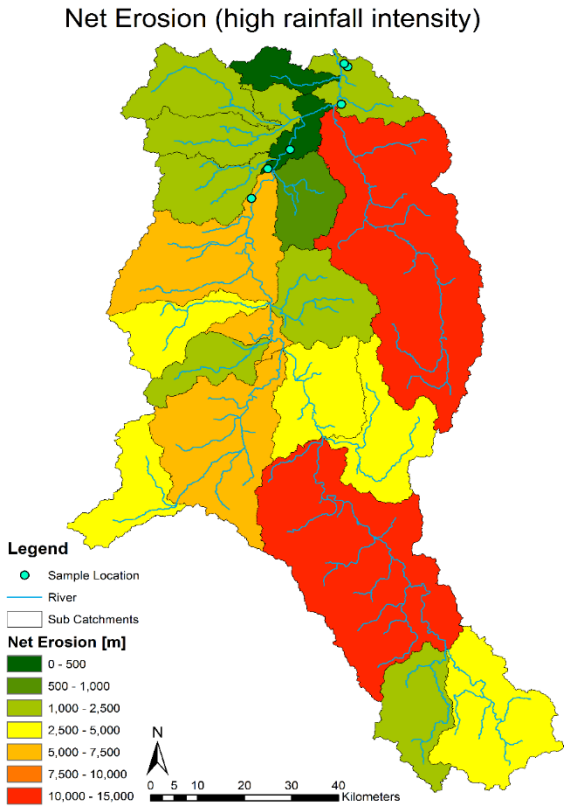

Figure 23. Net erosion per sub catchment for the high rainfall intensity scenario.

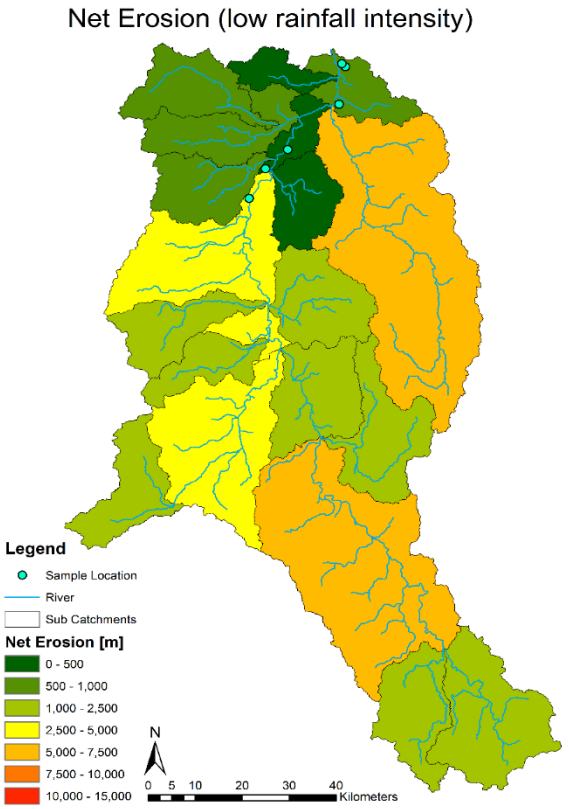

Figure 24. Net erosion per sub catchment for the low rainfall intensity scenario.

5. Discussion

The Allier river terrace Fx_{III} has shown to be difficult to date. A reliable age is needed to deduce the evolution of the river catchment. With the information shown in the previous chapters, I will be able to analyse the new ages for this terrace and compare these to the OSL tracing and LAPSUS results. To do this properly, I will first answer my sub questions:

- *Is it possible to use three OSL tracing techniques on the Fx_{III} terrace level of the Allier river?*

It is possible to use the three OSL-tracing techniques on this terrace level, but there are some difficulties. The lack of suitable quartz makes it hard to complete the bleaching index and to get quartz-ages. Feldspar provides a good alternative, although more research is needed on for example feldspar sensitivity before it can be used independently.
The incomplete Bleaching Index (BI) was not a problem for this research, since all samples were alike. When samples are very different incompleteness can be a bigger problem, since the BI really is dependent on the normalizing factor. Feldspar is not best suitable because of possible instabilities, such as incomplete bleaching and anomalous fading.

Though there are some troubles with the techniques, each separate technique did provide useful information:

- Bleaching analysis was used to indicate transport dynamics or differences therein, but all 6 samples performed roughly the same in the bleaching index. The bleaching conditions are therefore comparable. The original use of the BI is to look whether a sample is poorly bleached. However, because the normalisation to quartz could not be done, it is arguable whether it is possible to determine the amount of poor bleaching for the six samples.
- Sensitivity performed not as expected. I expected sensitivity to increase further downstream due to more burial-irradiation cycles (Pietsch et al., 2008; Sawakuchi et al., 2011), but in this terrace level the sensitivity decreases. This could mean that a (shorter) tributary might influence the sensitivity of the downstream part of the Fx_{III} terrace level, or that other processes than burial-irradiation cycles might be more important for change in sensitivity.
  Pietsch et al. (2008) state that they found this increase in sensitivity in an ephemeral river in Australia, which results in multiple burial and irradiation cycles because the river runs dry every year. The Allier river transports water year-round, so chances for repeated burial and irradiation are smaller, which would reduce the increase in sensitivity. However, Sawakuchi et al. (2011) find also a small increase in sensitivity in the sediments from a river in south-eastern Brazil, which transports water year-round as well.
  The tributaries of the Allier might have different fluvial characteristics compared to the main river, for example more turbid or more stream power. This can provide a change in the amount of burial-irradiation cycles compared to the main river.
  Sawakuchi et al. (2018) provide an alternative solution by stating that the sensitivity is dependent on the source material. This could also be the case for the Allier sediments, since differences in lithology are present in the Allier catchment, such as granites, basalts and Oligocene marls, clays and sandstones (Lucazeau et al., 1984) (figure 1).
- Feldspar heterogeneity provided the OD, which showed bioturbation in sample 187. This is of great importance in the eventual age determination. Though the feldspar heterogeneity proved to be useful, quartz heterogeneity might have provided even more information. Since quartz bleaches faster than feldspar, it is better able to show differences in bleaching due to for instance depositional circumstances or transport. Unfortunately it was not possible in this research to compare feldspar and quartz heterogeneity, but it could be interesting for further research.

- *Can we see differences in the fluvial dynamics between the six sampled locations?*

Sensitivity analysis provided a difference between the upstream and downstream samples, as explained above. Bleaching rate analysis and the heterogeneity of the D_e-distribution, both used for bleaching differences, did show a clear difference between bioturbated and non-bioturbated samples. The non-bioturbated samples all showed similar amounts of poor bleaching. This could mean that the processes responsible for bleaching are roughly the same for all samples. Combining this with the change in sensitivity downstream, which might suggest a hypothetical change in transport distance, it would be possible that the way of transport does not seem to influence the degree of bleaching in the six samples. This possibility was not expected, because it is believed that most fluvial samples are partly bleached due to the transport in the river (Wallinga, 2002). An alternative explanation of the change in sensitivity and similar bleaching conditions might be that the river and tributaries all have similar ways of transport providing similar bleaching conditions, but that the source of the sediment changes. However, it is not likely that all tributaries of the Allier have the same fluvial characteristics. The following questions will elaborate more on this subject.

- *What information can LAPSUS provide to this research?*
LAPSUS shows that two areas are important sediment suppliers to the Allier river. The southern catchment, which is in fact part of the Allier itself but will be called Langeac to the largest city within this catchment, shows highest values of SDR and net erosion, indicating that in this large area almost all eroded sediments flow to the Allier. The north-eastern catchment, which is the tributary the Dore (figure 1), also has a high net erosion, but the SDR is a little bit lower compared to the southern catchments. This means that there is more sedimentation taking place within the Dore catchment, indicating a difference in river characteristics compared to the Langeac sub catchment.
In the Langeac catchment sandstones are present (Lucazeau et al., 1984) and the Dore flows through granite (figure 1). Other catchments with higher sediment contributions are linked to the western rift shoulder, where volcanic material like basalts and lava flows are abundant. However, the LAPSUS model was not calibrated and all parameter values were set to default, except for the elevation and flow accumulation. The amounts of erosion shown in figures 23 & 24 are therefore solely dependent on the slope and the amount of water flowing through the sub catchments. These maps give therefore only a first indication of what the sub catchments can provide to the Allier river. If the LAPSUS model will be used for further research, it might be recommendable to use at least differences in lithology, since it is known that these differences are present (figure 1).
I expect that the absolute amounts of erosion and sedimentation will change when implementing lithology in the model, but the relative importance will remain the same. The Dore and Langeac sub catchments are the largest sub catchments and therefore have the largest area to erode, so the relative amount of eroded sediments compared to the smaller neighbouring catchments will still be higher. For further analysis I will therefore assume that the amount of water and the slope are indeed the major factors for erosion, so the net erosion maps can be used to determine the erosional patterns in the Allier catchment.

- *How do the methods results (OSL and LEM) compare to each other?*
The sediment in the upstream samples most likely originates from the Langeac clay, marl and sandstone area (Lucazeau et al., 1984). OSL measurements are done on the sand fraction (212-250 µm), so the material that I used probably stems from the sandstones in that area. Quartz from sandstones is sensitive in OSL measurements (Jeong & Choi, 2012), which can explain the sensitivity found in the upstream samples. The Dore erodes saprolite of granite, material that is deemed not sensitive to luminescence (Jeong & Choi, 2012; Reimann et al., 2017). The large influx of this material may be the reason a drop in sensitivity in the quartz grains is found. The connection with the western rift shoulder in some sub catchments indicates where the darker basaltic material probably originates.
Next to the different source material of the sediment, the difference in transport distance might also play a role in the sensitivity. The distance from the Langeac catchment to the regions with low SDR, i.e. more sedimentation compared to the Langeac catchment, is larger than from the Dore to the lower SDR regions. Jeong & Choi (2012) state that saprolite and freshly eroded granites have a low sensitivity, but the sensitivity increases after transportation, like we see for the downstream three samples. Saprolite quartz also is likely to be contaminated with feldspar (Reimann et al., 2017). This contamination is not easily removed, even by extensive etching. This contamination with feldspar is also found in sample 190, located just downstream of the confluence with the Dore.
The sensitivity change found for the six Fx_{III} samples is most probably a combination of the difference in source material and transport distance.

The SDR shows that some catchments have more erosion and/or less sedimentation than others, which can happen due to the differences in slope, but also due to differences in amount of water. The Langeac catchment for instance, has steep slopes, relatively large discharge (high value for maximum flow accumulation) and also a high SDR. In the flatter areas in the north, the amount of water increases in the Allier river and the SDR decreases, indicating more sedimentation compared to erosion. This change in SDR implies different river characteristics, like turbidity and stream power. If we assume that the material in the upstream 3 samples stems from the area of Langeac in the south, and the material from the downstream 3 samples mostly from the Dore, it could be hypothesised that at least a minor difference in river dynamics would take place due to slope, discharge differences and SDR. However, the bleaching analysis showed that all samples have similar amounts of poor bleaching. This again indicates that bleaching maybe does not occur in transport (Wallinga, 2002), but perhaps already before erosion (e.g. on erosional slopes) or after deposition (e.g. as top layer on the newly forming terrace) by the river. Both the OSL tracing combination of sensitivity and BI and the combination of LAPSUS and BI indicate that bleaching might not occur in transport, but more research is needed on this topic to identify what really happens with the sediments in a river, and how that contributes to bleaching.

- What is the age of terrace level Fx_{III}?

Before I am able to explain the landscape evolution, decisions should be made on the age of the terrace level Fx_{III}. Figure 25 shows all ages measured before, including the CAM-225 ages I measured in this research, except the age range of sample 187.

As can be seen in this figure, the new ages are partly consistent with previous work. Sample 177 and 180 are comparable with the quartz as well as the Multiple Grain feldspar measurements. These ages are therefore very reliable. Sample 182 is just within 1σ of the older SG feldspar measurement.

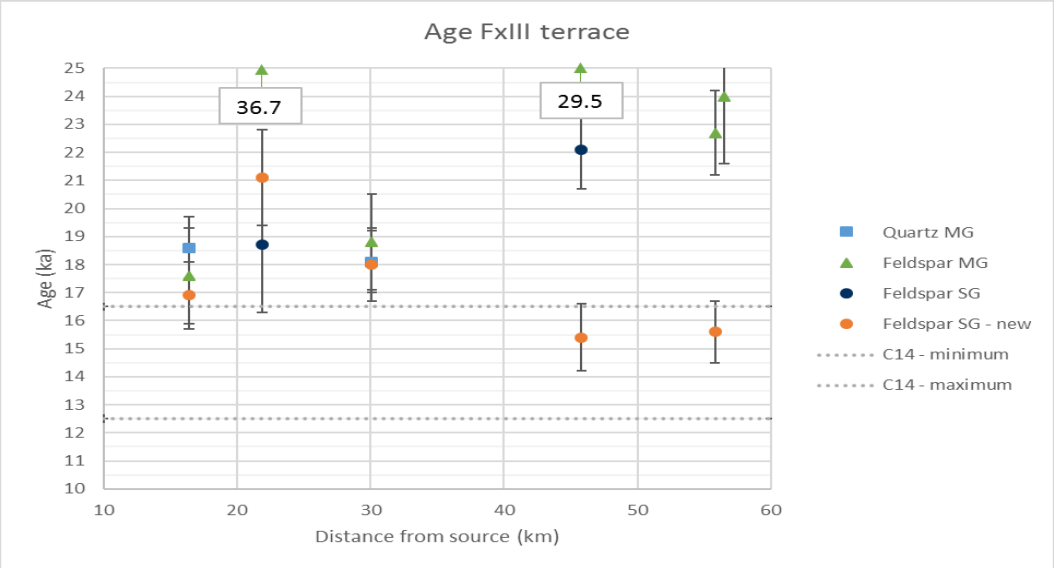

Figure 25. All ages determined for the Fx_{III} river terrace. Samples are displayed from upstream to downstream (-177, -182, -180, -190, -188, -187). The numbered boxes show two ages found with MG feldspar measurements, but due to readability reasons these are not plotted.

To explain why these measurements, which are both SG feldspar, are different, I came up with the following:

1. The measurement protocol differs. Both were pIRIR measurements, but in the new protocol three SG measurements were done, while the old protocol only did one SG measurement after a whole disc stimulation. The measurement temperature is the same (225°C).
2. The older measurement consists of more suitable grains (49 compared to 31), which makes this older measurement more trustworthy. The OD of both measurements is the same.
3. The BI is highest for this sample. As explained before, this could mean that there is an offset in age, implying that this sample should actually be younger than we date it.
4. The new measurement includes a fading a residual dose correction, while the old measurement does not include this. If we assume that the correction for the new measurement can be used for the old measurement (which is a bold assumption, since this depends on the measurement protocol, which is very different) it would mean that the old measurement gets even younger.

After taking this into account, I suggest to use the old SG measurement for sample 182, mostly because of the higher number of grains used and the indication of the BI that the age should probably be lower than measured. The precision is lower for this sample, but since it is within 1σ of the other upstream samples I believe this age represents the age of the terrace level better.

Sample 190 also has an older SG feldspar measurement, but the old and new sample are not within 1σ of each other. The old measurement was marked as questionable by the researcher (appendix A1), so for this sample I will use the newly measured age.

The multiple grain feldspar measurements are not comparable with the SG measurements, because the MG include the outliers. These outliers have a huge impact on the final equivalent dose, which makes these ages inaccurate. Sample 177 and 180 do not have as much outliers (in the non-iterated dataset, appendix A3), which is why these MG measurements are comparable with the SG measurements. Furthermore, the MG are measured on a temperature of 290°C, which has a higher residual dose than the SG measurements (10 ± 5 Gy), increasing the error tremendously. The MG measurement is also more sensitive to incomplete bleaching. All ages for the different samples can be found in appendix A1, the ages that I have decided on are shown in table 8.

Table 8. Final age of the Fx_{III} terrace samples.

Age per sample (ka)	
177	16.91 ± 1.2
182	18.70 ± 2.4
180	17.99 ± 1.3
190	15.37 ± 1.2
188	15.57 ± 1.1

The upstream samples are not consistent with the ^{14}C dating on charcoal and nearby lacustrine sediments done by Veldkamp and Kroonenberg (1993), while the downstream samples are. The upper uncalibrated ^{14}C date, 16.6 ± 0.25 ka, is based on charcoal fragments in a cryoturbated paleosol in the Fx_I terrace level below the Fx_{III}, upstream of the confluence of the Dore. This fragment is found near Maringues, close to the confluence of the La Morge with the Allier river (figure 1). If one would assume that Fx_{III} is synchronously deposited, it would mean that the charcoal entered the soil after formation of the Fx_{III} terrace and that the terrace level should be even younger than the current ^{14}C age suggests, or that one (or both) of the dating techniques is not correct. However, if one would assume that the terrace is not deposited synchronously but in separate events, it could mean that the upstream part of the terrace was already deposited when the charcoal entered the paleosol further downstream. The downstream part of the Fx_{III} terrace does seem to be younger, although all 5 samples are within 1σ of each other and thus might as well be of similar ages.

These results are very useful in reconstructing the evolution of the river terrace. In the following part I will use the tracing techniques and LAPSUS to answer the main question, which is:

When and how did the river landscape of the Allier catchment corresponding to terrace level Fx_{III} evolve?

When assuming synchronous deposition, an average age of 16.9 ka can be chosen for this terrace. 16.9 thousand years ago the last stadial of the Late Weichselian dominated the climate (Beaulieu et al., 1994). The climate had not yet started changing, so river terrace build up due to ice melt in a warming climate was probably not the case. However, eruptions of volcanoes in the western rift shoulder could have induced terrace formation by melting the ice overlying the volcano.
A well-researched volcano is the Tartaret volcano (figure 26), which erupted around 16.4 ± 2.4 ka (van Kapel MSc thesis, 2018; pers. com. Tony Reimann, 2019). This age is based on only one sample of scoria, and although there was not a lot of material (resulting in a large error), the performance of this sample is acceptable. Figure 27 shows the terrace ages and the age range of the scoria dating. This eruption can also explain the presence of basaltic material in the terrace level, since it lies within one of the sub catchments with a higher SDR and a high net erosion (figure 23 and 24).
Other studies on this volcano reveal 24 mentioned dates of eruptions (Bastin, Gewelt, & Juvigné, 1990; Brousse, Maury, & Santoire, 1976; Guérin, 1983; Macaire et al., 1992; Pilleyre et al., 1992). The ages resulting from these studies range from 7700 ± 500 BP (Brousse et al., 1976) till 28200 ± 2300 years old (Guérin, 1983). Many of these ages were acquired using outdated techniques and uncertainties remain on the material that was dated, since it is not always clear that the material really originates from the Tartaret volcano.
Not only the Tartaret volcano was active around 16.9 thousand years ago. According to Nowell et al. (2006) many eruptions occurred roughly at the same time in the Massif Central. Eight different eruptions have been dated within the time span of the new OSL SG feldspar dates, 15.4-18.7 thousand years ago. The locations of the dated material (tephra or lava flows) are shown in figure 24. All available material has been dated with Thermo Luminescence, except one lava flow that was dated with ^{14}C, although it is not stated on what material this dating exactly is performed.

The abundance of volcanic eruptions makes clear that it is likely that the material in the Allier Fx_{III} terrace originates not only from one volcano like the Tartaret, but from multiple volcanoes on the western rift shoulder. It would be a nice follow-up research to study the eruptions mentioned by Nowell et al. (2006) and update the ages by using newer techniques. Also the mineral content of the lava flows can be compared to the basaltic material in the Fx_{III} terrace level, to deduce where the material comes from. A first indication of the mineral content of the Fx_{III} terrace shows that the percentage of basaltic components increases towards the Morge tributaray (figure 1), but decreases after confluence with the Dore (pers. com. Veldkamp, 2019), indicating that the Dore indeed influences the sediment composition of the downstream Allier river terraces, but also that the amount of basaltic material builds up in the sediment before the confluence of the Dore. The change in

mineral content corresponds to the results of the sensitivity analysis, where sensitivity drops after confluence of the Dore, presumably due to the occurrence of insensitive granite and saprolite. The accumulation of the basaltic material can be explained with inflow of basaltic material more upstream, for example in the catchment of La Morge river (figure 1).

Considering all arguments presented, still not a sole answer can be given to the main question. The three hypotheses formed for this area were synchronous deposition in a single or in multiple events, or diachronous deposition.
The SG feldspar ages are all within 1σ of each other, indicating synchronous deposition due to a single event. The change in sensitivity and the mineral composition indicate the great importance of the Dore tributary to the Fx_{III} terrace, proving that tributary mixing indeed can be one of the causes for the change in age observed in this and former research. Also, multiple volcanic events can be held responsible for the contribution of basaltic material to the terrace. Therefore the two hypotheses about synchronous deposition might both be true. The idea of diachronous deposition can most likely be rejected, since climate change had not yet started (Beaulieu et al., 1994) and all results point towards synchronous deposition. Still, further research is needed to explore the origin of the material present in the Fx_{III} terrace.

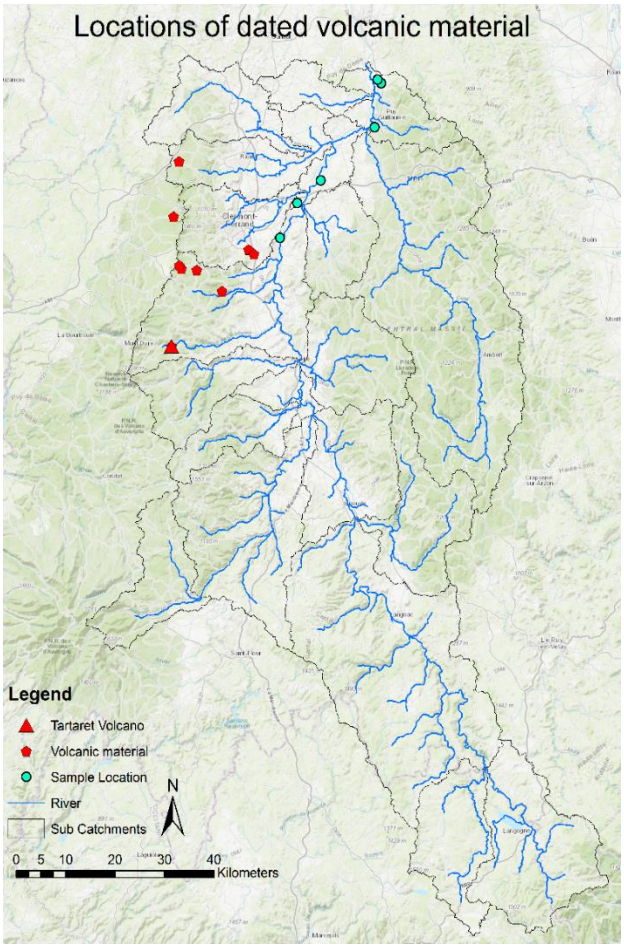

Figure 26. Catchment of the Allier river, including sampling points and location of dated volcanic material such as tephra and lava flows. Exact coordinates of the shown locations can be found in the paper of Nowell et al. (2006)

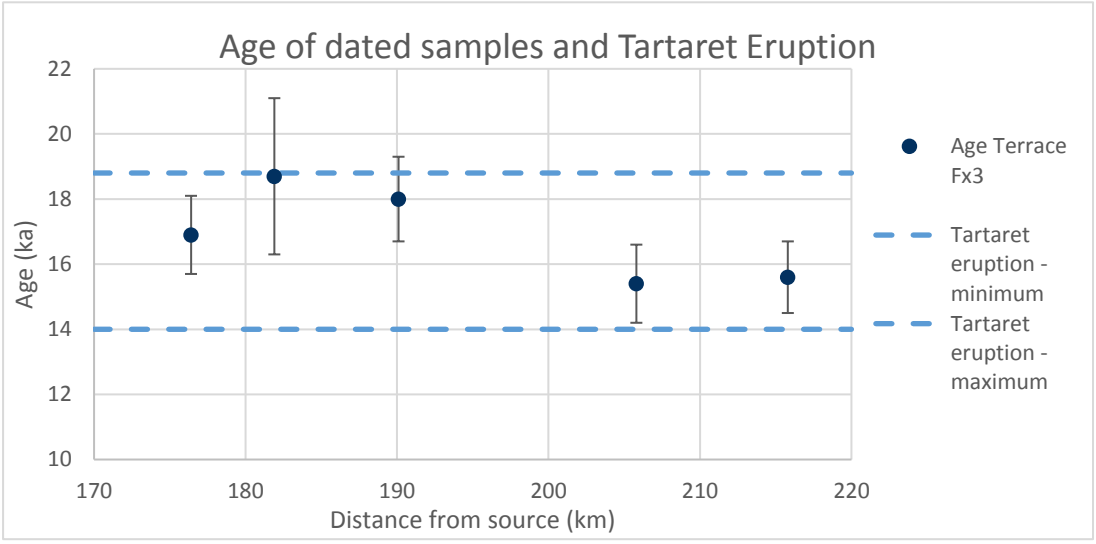

Figure 27. Ages of terrace level Fx_{III} and the minimum and maximum age of the Tartaret volcano eruption.

6. Conclusion

The bleaching analysis (BI) and the analysis of the heterogeneity of the D_e distribution (OD) provided similar results for all five non-bioturbated samples, but a change in quartz sensitivity was found between three upstream and two downstream samples. This can be an indication of the following causes: the source material and thus base sensitivity is different, or the transport distance or way of transport is different, resulting in a different amount of burial-irradiation cycles. When this change originates from difference in source material, it could mean that all samples experienced the same way of transport, otherwise larger differences in OD and BI would have been found. If the change in sensitivity originates from differences in transport distance or way of transport, it would mean that bleaching might not occur in transport, but on erosional slopes or after deposition. Next to that, the slope and SDR maps from LAPSUS show that sub catchments probably had different river dynamics, with changes in sediment delivery ratio and differences in discharge. Combining this with the lack of change in poor bleaching between the samples, this looks to be the second indication that bleaching of the sediment does not occur in transport.

The net erosion maps from LAPSUS are used to determine whether the sensitivity change originates from differences in transport distance or source material. The maps showed that two sub catchments provide major amounts of sediment to the Allier river. The upstream source area, near Langeac, contains sandstones, which are sensitive to OSL. The downstream source area, the Dore tributary, contains granite and saprolite of granite, which is deemed not sensitive to OSL. These source materials are thought to be the major reason responsible for the change in sensitivity, indicating the importance of the Dore tributary during formation of terrace level Fx_{III}. The transport distance from these eroding areas towards the sample locations also is different, with greater distance from the Langeac area to the upstream sample locations compared to the Dore area to the downstream sample locations. The sensitivity change can therefore be explained by both differences in source material and transport distance.

The new dating of terrace level Fx_{III} resulted in an average age of 16.9 ka, with individual samples ranging between 15.4-18.7 ka. This means the formation of the terrace level took place in the last stadial of the Weichselian. Volcanism can induce terrace formation even in an ice age. Multiple volcanic eruptions are reported within the Allier catchment between 15.4-18.7 thousand years ago and will likely have influenced the Allier river terrace formation, explaining the darker colour of the sediment in terrace level Fx_{III}. The new dating is believed to be more accurate than before, but the processes for Fx_{III} terrace level formation are still not clearly defined. It might be caused by a single event like tributary mixing, it might be caused by multiple events like volcanic eruptions, but it might also still be caused by a combination of the two. More research on the area is therefore still needed to complete the history of evolution for the Allier catchment.

7. References

Armstrong, R. L. (Yale U., Leeman, W. P., & Malde, H. E. (1975). K--Ar dating quaternary and Neogene volcanic rocks of the Snake River Plain, Idaho. *Am. J. Sci.; (United States)*, *275:3*. https://doi.org/10.2475/ajs.275.3.225

Bailey, R. M., & Arnold, L. J. (2006). Statistical modelling of single grain quartz De distributions and an assessment of procedures for estimating burial dose. *Quaternary Science Reviews*, *25*(19), 2475–2502. https://doi.org/10.1016/j.quascirev.2005.09.012

Bastin, B., Gewelt, M., & Juvigné, E. H. (1990). A Propos de l'age et de l'origine des tephras tardiglaciaires T4 et T5 de Godivelle-Nord (Massif Central, France). *Annales de La Société Géologique de Belgique*, 165–178.

Beaulieu, J.-L. de, Andrieu, V., Ponel, P., Reille, M., & Lowe, J. J. (1994). The Weichselian Late-glacial in southwestern Europe (Iberian Peninsula, Pyrenees, Massif Central, northern Apennines). *Journal of Quaternary Science*, *9*(2), 101–107. https://doi.org/10.1002/jqs.3390090203

Berendsen, H. J. A., & Stouthamer, E. (2000). Late Weichselian and Holocene palaeogeography of the Rhine–Meuse delta, The Netherlands. *Palaeogeography, Palaeoclimatology, Palaeoecology*, *161*(3), 311–335. https://doi.org/10.1016/S0031-0182(00)00073-0

Boenigk, W. (1995). Middle Pleistocene terrace stratigraphy of the lower and middle Rhine. *Mededelingen - Rijks Geologische Dienst*, *52*, 71–87. Retrieved from Scopus.

Bonnet, S., Reimann, T., Wallinga, J., Lague, D., davy, P., & Lacoste, A. (In Review). *Landscape dynamics revealed by luminescence signals of feldspars from fluvial terraces*.

Broers MSc thesis, A. (2016). *Luminescence dating of River terraces of the Allier, Massif-Central, France*. Wageningen University of Research.

Brousse, R., Maury, R. C., & Santoire, J. P. (1976). L'âge de la coulée du Tartaret. *Comptes Rendus de l'Académie Des Sciences Paris*, *282*, 1618–1620.

Bull, W. B. (1990). Stream-terrace genesis: implications for soil development. *Geomorphology*, *3*(3), 351–367. https://doi.org/10.1016/0169-555X(90)90011-E

Burow, C. (2018a). calc_CentralDose(): Apply the Central age model (CAM) after Galbraith et al. (1999) to a given De distribution (Version 1.3.2).

Burow, C. (2018b). calc_FiniteMixture(): Apply the finite mixture model (FMM) after Galbraith (2005) to a given De distribution (Version 0.4).

Burow, C. (2018c). calc_MinDose(): Apply the (un-)logged minimum age model (MAM) after Galbraith et al. (1999) to a given De distribution (Version 0.4.4).

Chamberlain, E. L., Wallinga, J., Reimann, T., Goodbred, S. L., Steckler, M. S., Shen, Z., & Sincavage, R. (2017). Luminescence dating of delta sediments: Novel approaches explored for the Ganges-Brahmaputra-Meghna Delta. *Quaternary Geochronology*, *41*, 97–111. https://doi.org/10.1016/j.quageo.2017.06.006

Cubizolle, H., Valadas, B., Gagnaire, J., & Evin, J. (2001). La dynamique des versants dans le bassin de la Dore durant la deuxième moitié de l'Holocène {Massif central, France) ; premières données géoarchéologiques et datations radiocarbone / The dynamics of slopes in the catchment of the Dore during the Late Holocene (Massif central, France) : preliminary geoarchaeological data and radiocarbone dating. *Quaternaire*, *12*(1), 15–29. https://doi.org/10.3406/quate.2001.1678

Cunningham, A., Wallinga, J., Hobo, N., Versendaal, A., Makaske, B., & Middelkoop, H. (2015). Re-evaluating luminescence burial doses and bleaching of fluvial deposits using Bayesian computational statistics. *Faculty of Science, Medicine and Health - Papers: Part A*, 55–65. https://doi.org/10.5194/esurf-3-55-2015

Dietze, M., & Kreutzer, S. (2018a). plot_KDE(): Plot kernel density estimate with statistics (Version 3.5.7).

Dietze, M., & Kreutzer, S. (2018b). plot_RadialPlot(): Function to create a Radial Plot (Version 0.5.5).

Duller, G. (2015). Risoe Luminescence Analyst (Version 4.31.9) [English]. Aberystwyth: Aberystwyth University.

Eden, D. N., Palmer, A. S., Cronin, S. J., Marden, M., & Berryman, K. R. (2001). Dating the culmination of river aggradation at the end of the last glaciation using distal tephra compositions, eastern North Island, New Zealand. *Geomorphology*, *38*(1), 133–151. https://doi.org/10.1016/S0169-555X(00)00077-5

Guérin, G. (1983). *La thermoluminescence des plagioclases: méthode de datation du volcanisme: applications au domaine volcanique français: Chaîne des Puys, mont Dore et Cezallier, Bas Vivarais.* Université Pierre et Marie Curie.

Harmand, D., & Cordier, S. (2012). The Pleistocene terrace staircases of the present and past rivers downstream from the Vosges Massif (Meuse and Moselle catchments). *Netherlands Journal of Geosciences*, *91*(1–2), 91–109. https://doi.org/10.1017/S0016774600001529

Huntley, D. J., Godfrey-Smith, D. I., & Thewalt, M. L. W. (1985). Optical dating of sediments. *Nature*, *313*(5998), 105–107. https://doi.org/10.1038/313105a0

Huntley, D. J., & Lamothe, M. (2001). Ubiquity of anomalous fading in K-feldspars and the measurement and correction for it in optical dating. *Canadian Journal of Earth Sciences*, *38*(7), 1093–1106. https://doi.org/10.1139/e01-013

Jenson, S. K., & Domingue, J. O. (1988). Extracting topographic structure from digital elevation data for geographic information system analysis. Photogrammetric Engineering and Remote. *Sensing*, *54*, 1593–1600.

Jeong, G. Y., & Choi, J.-H. (2012). Variations in quartz OSL components with lithology, weathering and transportation. *Quaternary Geochronology*, *10*, 320–326. https://doi.org/10.1016/j.quageo.2012.02.023

Kreutzer, S. (2018). calc_FadingCorr(): Apply a fading correction according to Huntley & Lamothe (2001) for a given g-value and a given tc (Version 0.4.2).

Kreutzer, S., Burow, C., Dietze, M., Fuchs, M. C., Schmidt, C., Fischer, M., & Friedrich, J. (2018). Comprehensive Luminescence Dating Data Analysis R (Version 0.8.6) [English].

Litchfield, N. J., & Clark, K. J. (2015). Fluvial terrace formation in the lower Awhea and Pahaoa River valleys, New Zealand: implications for tectonic and sea-level controls. *Geomorphology*, *231*, 212–228. https://doi.org/10.1016/j.geomorph.2014.12.009

López, G. I., Goodman-Tchernov, B. N., & Porat, N. (2018). OSL over-dispersion: A pilot study for the characterisation of extreme events in the shallow marine realm. *Sedimentary Geology*. https://doi.org/10.1016/j.sedgeo.2018.09.002

Lu, H., Moran, C. J., & Prosser, I. P. (2006). Modelling sediment delivery ratio over the Murray Darling Basin. *Environmental Modelling & Software*, *21*(9), 1297–1308. https://doi.org/10.1016/j.envsoft.2005.04.021

Lucazeau, F., Vasseur, G., & Bayer, R. (1984). Interpretation of heat flow data in the french massif central. *Tectonophysics*, *103*(1), 99–119. https://doi.org/10.1016/0040-1951(84)90077-5

Macaire, J. J., Cocirta, C., De Luca, P., Gay, I., & de Goër de Hervé, A. (1992). Origins, Ages and Evolution of the Tardi- and Postglacial Lacustrine Systems in the'Lac Chambon' Basin(Puy-de-Dome, France)(Origines, Ages et Evolution des Systemes Lacustres Tardi- et Postglaciaires dan le bassin du lac Chambon(Puy-de-Dome, France)). *Comptes Rendus de l'Académie Des Sciences Paris*, *315*(9).

Nowell, D. A. G., Jones, M. C., & Pyle, D. M. (2006). Episodic Quaternary volcanism in France and Germany. *Journal of Quaternary Science*, *21*(6), 645–675. https://doi.org/10.1002/jqs.1005

Parmenter, W. B., & Melcher, J. (2012). *Watershed and Drainage Delineation by Pour Point in ArcMap 10*. 16.

Pastre, J. F. (1987). *Les formations Plio-Quaternaires dus bassin de l'Allier et le volcanisme régional (Massif Central français).* (PhD thesis). Paris VI Pierre et Marie Curie, Paris.

Pastre, J. F. (2004). The Perrier Plateau: a plio-pleistocene long fluvial record in the river Allier Basin, Massif Central, France. *Quaternaire*, *15*(1–2), 87–101.

Pastre, J. F. (2005). Les nappes alluviales de l'Allier en Limagne (Massif Central, France) : stratigraphie et corrélations avec le volcanisme régional. *Quaternaire*, (vol. 16/3), 153–175. https://doi.org/10.4000/quaternaire.383

Pietsch, T. J., Olley, J. M., & Nanson, G. C. (2008). Fluvial transport as a natural luminescence sensitiser of quartz. *Quaternary Geochronology*, *3*(4), 365–376. https://doi.org/10.1016/j.quageo.2007.12.005

Pilleyre, Th., Montret, M., Fain, J., Miallier, D., & Sanzelle, S. (1992). Attempts at dating ancient volcanoes using the red TL of quartz. *Quaternary Science Reviews*, *11*, 13–17.

Porat, N. (2006). *Use of magnetic separation for purifying quartz for luminescence dating*. *24*, 4.

Preusser, F., Degering, D., Fuchs, M., Hilgers, A., Kadereit, A., Klasen, N., … Spencer, J. Q. G. (2008). Luminescence dating: basics, methods and applications. *Quaternary Science Journal*, *57*(1–2), 95–149.

Reimann, T., Notenboom, P. D., De Schipper, M. A., & Wallinga, J. (2015). Testing for sufficient signal resetting during sediment transport using a polymineral multiple-signal luminescence approach. *Quaternary Geochronology*, *25*, 26–36. https://doi.org/10.1016/j.quageo.2014.09.002

Reimann, T., Román-Sánchez, A., Vanwalleghem, T., & Wallinga, J. (2017). Getting a grip on soil reworking – Single-grain feldspar luminescence as a novel tool to quantify soil reworking rates. *Quaternary Geochronology*, *42*, 1–14. https://doi.org/10.1016/j.quageo.2017.07.002

Reimann, T., Thomsen, K. J., Jain, M., Murray, A. S., & Frechen, M. (2012). Single-grain dating of young sediments using the pIRIR signal from feldspar. *Quaternary Geochronology*, *11*, 28–41. https://doi.org/10.1016/j.quageo.2012.04.016

Reimann, T., Tsukamoto, S., Naumann, M., & Frechen, M. (2011). The potential of using K-rich feldspars for optical dating of young coastal sediments – A test case from Darss-Zingst peninsula (southern Baltic Sea coast). *Quaternary Geochronology*, *6*(2), 207–222. https://doi.org/10.1016/j.quageo.2010.10.001

Sawakuchi, A. O., Blair, M. W., DeWitt, R., Faleiros, F. M., Hyppolito, T., & Guedes, C. C. F. (2011). Thermal history versus sedimentary history: OSL sensitivity of quartz grains extracted from rocks and sediments. *Quaternary Geochronology*, *6*(2), 261–272. https://doi.org/10.1016/j.quageo.2010.11.002

Sawakuchi, A. O., Guedes, C. C. F., DeWitt, R., Giannini, P. C. F., Blair, M. W., Nascimento, D. R., & Faleiros, F. M. (2012). Quartz OSL sensitivity as a proxy for storm activity on the southern Brazilian coast during the Late Holocene. *Quaternary Geochronology*, *13*, 92–102. https://doi.org/10.1016/j.quageo.2012.07.002

Sawakuchi, A. O., Jain, M., Mineli, T. D., Nogueira, L., Bertassoli, D. J., Häggi, C., … Cunha, D. F. (2018). Luminescence of quartz and feldspar fingerprints provenance and correlates with the source area denudation in the Amazon River basin. *Earth and Planetary Science Letters*, *492*, 152–162. https://doi.org/10.1016/j.epsl.2018.04.006

Schoorl, J. M., Sonneveld, M. P. W., & Veldkamp, A. (2000). Three-dimensional landscape process modelling: the effect of DEM resolution. *Earth Surface Processes and Landforms*, *25*(9), 1025–1034. https://doi.org/10.1002/1096-9837(200008)25:9<1025::AID-ESP116>3.0.CO;2-Z

Schumm, S. A. (1993). River Response to Baselevel Change: Implications for Sequence Stratigraphy. *The Journal of Geology*, *101*(2), 279–294. https://doi.org/10.1086/648221

Tarboton, D. G., Bras, R. L., & Rodriguez-Iturbe, I. (1991). On the extraction of channel networks from digital elevation data. *Hydrological Processes*, *5*(1), 81–100. https://doi.org/10.1002/hyp.3360050107

Taylor, D. M., Griffiths, H. I., Pedley, H. M., & Prince, I. (1994). Radiocarbon-dated Holocene pollen and ostracod sequences from barrage tufa- dammed fluvial systems in the White Peak, Derbyshire, UK. *The Holocene*, *4*(4), 356–364. https://doi.org/10.1177/095968369400400403

Thomsen, K. J., Murray, A. S., Jain, M., & Bøtter-Jensen, L. (2008). Laboratory fading rates of various luminescence signals from feldspar-rich sediment extracts. *Radiation Measurements*, *43*(9), 1474–1486. https://doi.org/10.1016/j.radmeas.2008.06.002

van Kapel MSc thesis, L. (2018). *Geomorphological analysis of the interaction between glaciation and the Tartaret volcano in the late quaternary in the Lac Chambon region, France*. Wageningen University of Research.

Veldkamp, A., & Kroonenberg, S. B. (1993). Late Quaternary chronology of the Allier terrace sediments (Massif Central, France). *Netherlands Journal of Geosciences*, *72*, 179–192.

Veldkamp, T. (1991). *QUATERNARY RIVER TERRACE FORMATION IN THE ALLIER BASIN, FRANCE.* Wageningen.

Veldkamp, T., Schoorl, J. M., & Viveen, W. (2016). Predicting reach-specific properties of fluvial terraces to guide future fieldwork. A case study for the Late Quaternary River Allier (France) with the FLUVER2 model. *Earth Surface Processes and Landforms*, *41*(15), 2256–2268. https://doi.org/10.1002/esp.4042

Wallinga, J. (2002). Optically stimulated luminescence dating of fluvial deposits: a review. *Boreas*, *31*(4), 303–322. https://doi.org/10.1111/j.1502-3885.2002.tb01076.x

Wallinga, J., Bos, A. J. J., Dorenbos, P., Murray, A. S., & Schokker, J. (2007). A test case for anomalous fading correction in IRSL dating. *Quaternary Geochronology*, *2*(1), 216–221. https://doi.org/10.1016/j.quageo.2006.05.014

Wintle, A. G. (1973). Anomalous Fading of Thermo-luminescence in Mineral Samples. *Nature*, *245*(5421), 143. https://doi.org/10.1038/245143a0

Appendix

A1 Previous work on Allier terrace levels

Village near Location Name	NCL Code	Client Code	Lat.	Lon.	Depth (m)	Palaeodose (Gy)	Doserate (Gy/ka)	Age (ka)	Validity	Comments
	Quartz ages									
Lempdes Top (Cournon)	NCL-2515177	AV15-01	45_45_32.9	3_13_05.2	5.3	57.4 ± 2.5	3.08 ± 0.13	18.6 ± 1.1	Likely OK	
Lempdes Lowest (Cournon)	NCL-2515178	AV15-02	45_45_32.9	3_13_05.2	14.4	122.7 ± 3.8	3.38 ± 0.15	36.3 ± 2.0	Likely OK	
Lempdes Middle (Cournon)	NCL-2515179	AV15-03	45_45_32.9	3_13_05.2	9.4	118.5 ± 9.5	3.51 ± 0.15	33.8 ± 3.1	Likely OK	
Culhat-Les Mouldeix	NCL-2515180	AV15-05		3_32_41.83	2	49.3 ± 2.3	2.73 ± 0.12	18.1 ± 1.1	Likely OK	
Les Martres-d'Artière mid	NCL-2515181	AV15-06	45_49_00.6	3_15_49.9	2	73.8 ± 5.3	2.76 ± 0.12	26.8 ± 2.3	Likely OK	
Les Martres-d'Artière top	NCL-2515182	AV15-07	45_49_00.6	3_15_49.9	1					no quartz signal
Les Martres-d'Artière low	NCL-2515183	AV15-08	45_19_07.4	3_15_50.9	11.1	59.7 ± 4.4	3.15 ± 0.14	18.9 ± 1.6	Likely OK	
Saint-Lazare (Maringues)	NCL-2515184	AV15-09	45_54_25.3	3_18_46.9	1.8	124.8 ± 32.5	3.88 ± 0.17	32.2 ± 8.5	Questionable	strange scater, close to saturation
Saint-Lazare (Maringues)	NCL-2515185	AV15-10	45_54_25.3	3_18_46.9	1.9					no quartz signal
Saint-Lazare (Maringues, quarry)	NCL-2515186	AV15-11	45_53_38.2	3_18_54.3	1.3					no quartz signal
Mariol (Northwest)	NCL-2515187	AV15-12	46_1_39.3	3_28_30.4	1.5		3.05 ± 0.13			too poor quartz signal
Mariol (Northwest)	NCL-2515188	AV15-13	46_1_35.8	3_28_59.9	0.5		3.43 ± 0.14			no quartz signal
Puy-Guillaume	NCL-2515189	AV15-14	45_57_00.3	3_27_55.8	1.9	80.4 ± 8.1	3.81 ± 0.17	21.1 ± 2.3	Likely OK	
Puy-Guillaume	NCL-2515190	AV15-15	45_57_00.3	3_27_55.8	0.8					no quartz signal
Les Vacherons (South), Chat Monroux	NCL-2515191	AV15-17	46_1_18.4	3_26_31.9	5.5	161.4 ± 6.2	3.61 ± 0.16	44.6 ± 2.6	Minimum age	quartz above saturation
	Feldspar multiple-grain ages									
Lempdes Top (Cournon)	NCL-2515177	AV15-01	45_45_32.9	3_13_05.2	5.3	71.0 ± 6.2	4.02 ± 0.17	17.6 ± 1.7	Likely OK	GOK, residual 10+/-5 Gy
Lempdes Lowest (Cournon)	NCL-2515178	AV15-02	45_45_32.9	3_13_05.2						no KF measurement
Lempdes Middle (Cournon)	NCL-2515179	AV15-03	45_45_32.9	3_13_05.2	9.4	214.0 ± 8.6	4.45 ± 0.18	48.1 ± 2.8	Doubtful	GOK, residual 10+/-5 Gy
Culhat-Les Mouldeix	NCL-2515180	AV15-05		3_32_41.83	2	69.0 ± 5.7	3.67 ± 0.15	18.8 ± 1.7	Likely OK	GOK; residual 10+/-5
Les Martres-d'Artière	NCL-2515181	AV15-06	45_49_00.6	3_15_49.9	2					no KF measurement
Les Martres-d'Artière	NCL-2515182	AV15-07	45_49_00.6	3_15_49.9	1	129.0 ± 15.7	3.51 ± 0.15	36.7 ± 4.7		GOK; residual 10 +/- 5 Gy
Les Martres-d'Artière	NCL-2515183	AV15-08	45_19_07.4	3_15_50.9	11.1	112.0 ± 6.9	4.09 ± 0.17	27.4 ± 2.0	Doubtful	GOK; residual 10 +/- 5 Gy
Saint-Lazare (Maringues)	NCL-2515184	AV15-09	45_54_25.3	3_18_46.9	1.8					no KF measurement

Saint-Lazare (Maringues)	NCL-2515185	AV15-10	45_54_25.3	3_18_46.9	1.9	843.0 ± 53.7	4.64 ± 0.19	181.8 ± 13.7	Likely OK	GOK, Residual 10 +/- 5 Gy
Saint-Lazare (Maringues, quarry)	NCL-2515186	AV15-11	45_53_38.2	3_18_54.3	1.3	546.0 ± 34.3	3.84 ± 0.16	142.1 ± 10.7	Likely OK	GOK, residual 10 +/- 5 Gy
Mariol (Northwest)	NCL-2515187	AV15-12	46_1_39.3	3_28_30.4	1.5	96.0 ± 8.7	3.99 ± 0.16	24.0 ± 2.4	Questionable	GOK, residual 10 +/- 5 Gy
Mariol (Northwest)	NCL-2515188	AV15-13	46_1_35.8	3_28_59.9	0.5	99.0 ± 5.4	4.37 ± 0.17	22.7 ± 1.5	Questionable	GOK, residual 10 +/- 5 Gy
Puy-Guillaume	NCL-2515189	AV15-14	45_57_00.3	3_27_55.8	1.9					no KF measurement
Puy-Guillaume	NCL-2515190	AV15-15	45_57_00.3	3_27_55.8	0.8	105.0 ± 5.0	4.50 ± 0.19	29.5 ± 1.9	Doubtful	GOK, residual 10 +/- 5 Gy
Les Vacherons (South), Chat Monroux	NCL-2515191	AV15-17	46_1_18.4	3_26_31.9	5.5	804.0 ± 19.5	4.55 ± 0.19	222.4 ± 11.4	Minimum age	GOK, residual 10 +/- 5 Gy, above saturation
Les Vacherons, Saint-Priest-Bramefant	NCL-2515192	AV15-18	46_1_18.4	3_26_31.9	4.4	1,546 ± 162	4.50 ± 0.18	344 ± 39	Questionable	GOK, residual 10 +/- 5 Gy, close to saturation
Coudes	NCL-2515193	AV15-19	46_1_18.4	3_26_31.9	2	888 ± 19	4.64 ± 0.20	191 ± 9	Minimum age	GOK, residual 10 +/- 5 Gy, above saturation
Cournon d'Auvergne	NCL-2515194	AV15-20	45_43_46.1	3_12_15.3	0.3	564 ± 69	3.88 ± 0.16	145 ± 19	Likely OK	GOK, residual 10 +/- 5 Gy
	Feldspar single grain									
Les Martres-d'Artière	NCL-2515182	AV15-07	45_49_00.6	3_15_49.9	1	62.9 ± 7.3	3.36 ± 0.18	18.7 ± 2.4		BS MAM, sigma_b 30+/-5 %, no fading correction
Puy-Guillaume	NCL-2515190	AV15-15	45_57_00.3	3_27_55.8	0.8	78.6 ± 3.7	4.35 ± 0.22	22.1 ± 1.4	Questionable	BS MAM, sigma_b 30+/-5, no fading correction

A2 Fading and residual dose correction

Fading

The fading measurement is based on the measurement protocol of the feldspar SG measurement (table 3). Below the times of fading can be seen. Within the table the time per step is noted. Run 15 is needed to make the fading time for all SG discs the same. Red cells indicate an error in the sequence: this irradiation step should not have been performed. This measurement is therefore not used in the calculation of the fading rate.

Fading time (s)	Run 1	Run 2	Run 3	Run 4	Run 5	Run 6	Run 7	Run 8	Run 9	Run 10	Run 11	Run 12	Run 13	Run 14	Run 15
	Irradiation*	Pre heat	Pause	IR50(SG)	IR150(SG)	IR225(SG)	Td irradiation	Cut heat	IR50(SG)	IR150(SG)	IR225(SG)	Bleaching	Irradiation	Pre heat	Pause
160	100	110		210	230	245	50	110	210	230	245	545	100	110	
12635				210	230	245	50	110	210	230	245	545			420
160	100	110		210	230	245	50	110	210	230	245	545	100	110	
	Pauze	180000													
192635				210	230	245	50	110	210	230	245	545			420
1000	100	110	840	210	230	245	50	110	210	230	245	545			
160	100	110		210	230	245	50	110	210	230	245	545	100	110	
12635	100	110		210	230	245	50	110	210	230	245	545			420
1000	100	110	840	210	230	245	50	110	210	230	245	545			

* Prompt irradiation. Fading time calculated as (Prompt/2 + Pre heat time)

Residual Dose

Samples were bleached for 70 hours in the SOL.
The protocol on the left tests what D_e a sample returns after given a D_e of 40 Gy. The protocol to the right determines the residual dose. Subtracted from each other the resulting dose should be 40 Gy.
This was true for all measurement temperatures.
The residual dose is then used to subtract from the sample D_e's for calculating the age. The residual doses are shown in table 6.

Both Fading and Residual Dose measurements were measured on samples (NCL-2515-) 177 and 190.

Step	Dose Recovery Feldspar SG protocol
1	Regenerative Dose*
2	Preheat of 250°C for 120.0s (5.00°C/s)
3	SG IRSL at 50°C for 2.0s
4	SG IRSL at 150°C for 2.0s
5	SG IRSL at 225°C for 2.0s
6	IR LED at 225°C for 500.0s (5.00°C/s)
7	Test dose (10 Gy)
8	Preheat of 250°C for 120.0s (5.00°C/s)
9	SG IRSL at 50°C for 2.0s
10	SG IRSL at 150°C for 2.0s
11	SG IRSL at 225°C for 2.0s
12	IR LED at 225°C for 500.0s (5.00°C/s)
	Repeat from step 1
	*Irradiation in the following order: 40Gy - 20Gy - 40Gy - 100Gy - 0Gy - 20Gy

Step	Residual Dose Feldspar SG protocol
1	Regenerative Dose*
2	Preheat of 250°C for 120.0s (5.00°C/s)
3	SG IRSL at 50°C for 2.0s
4	SG IRSL at 150°C for 2.0s
5	SG IRSL at 225°C for 2.0s
6	IR LED at 225°C for 500.0s (5.00°C/s)
7	Test dose (10 Gy)
8	Preheat of 250°C for 120.0s (5.00°C/s)
9	SG IRSL at 50°C for 2.0s
10	SG IRSL at 150°C for 2.0s
11	SG IRSL at 225°C for 2.0s
12	IR LED at 225°C for 500.0s (5.00°C/s)
	Repeat from step 1
	*Irradiation in the following order: 10Gy - 0Gy - 10Gy

A3 Radial Plots

Iterated data for the 50°C measurement

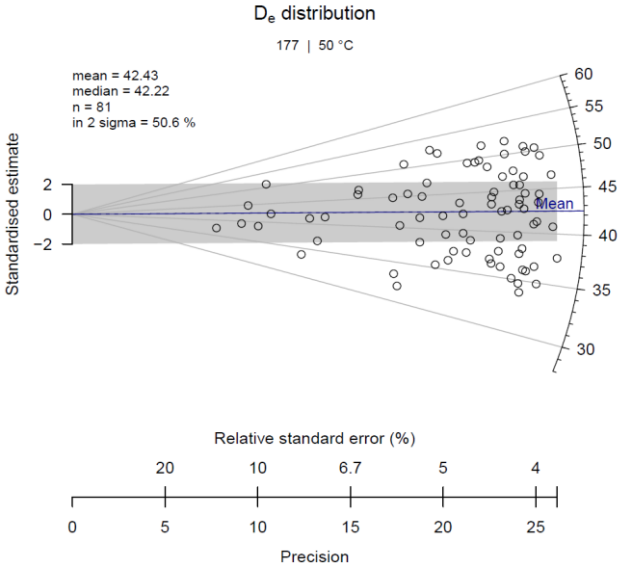

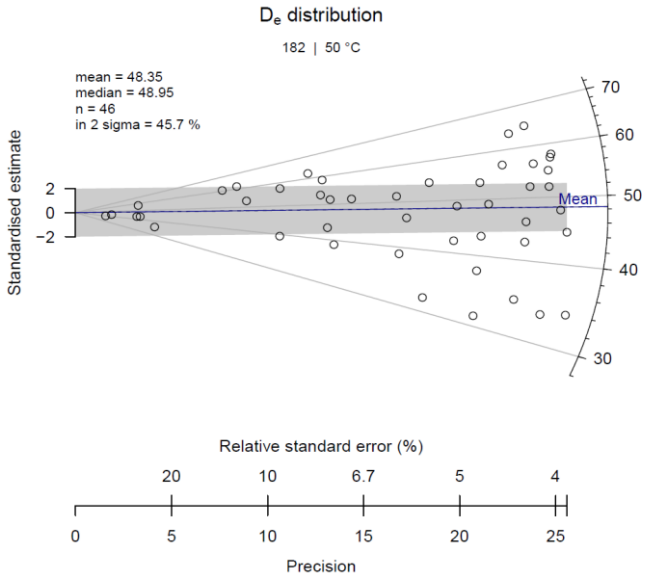

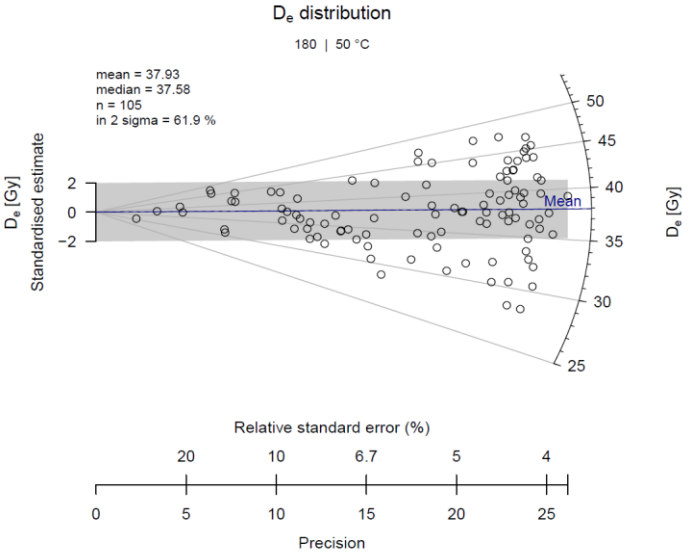

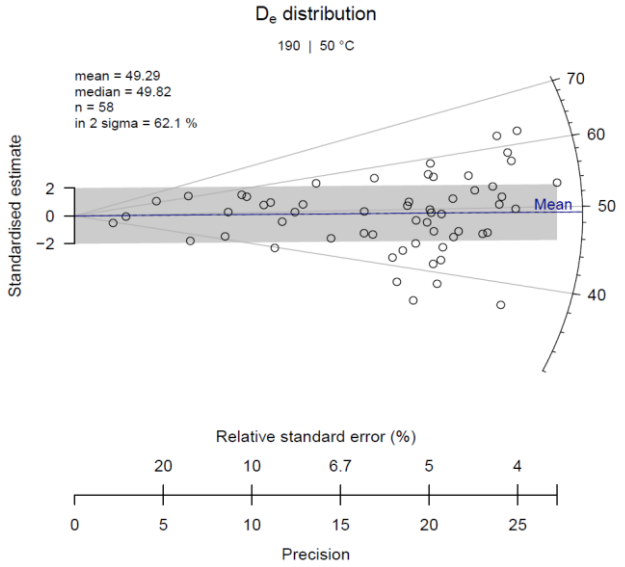

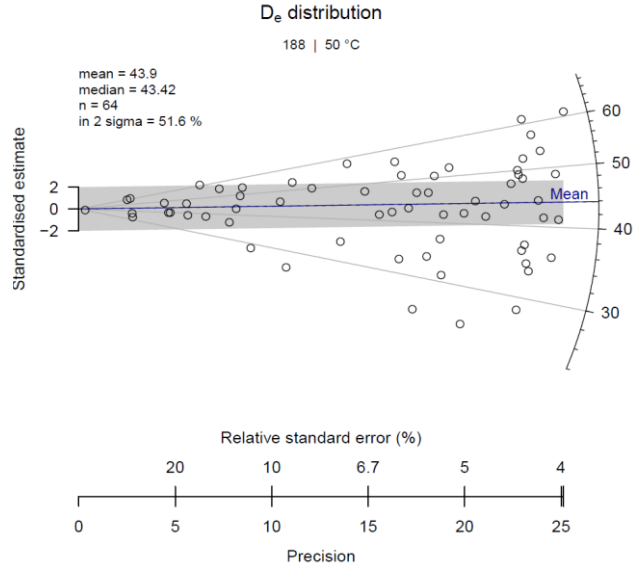

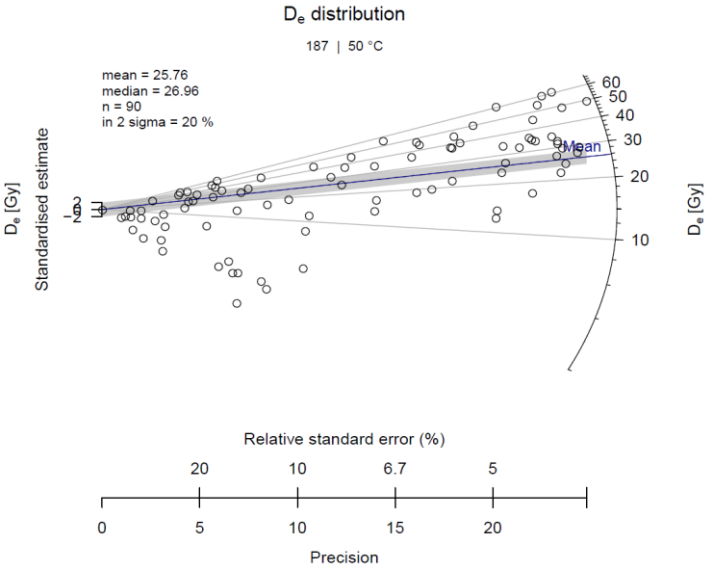

Original data of the 50°C measurement:

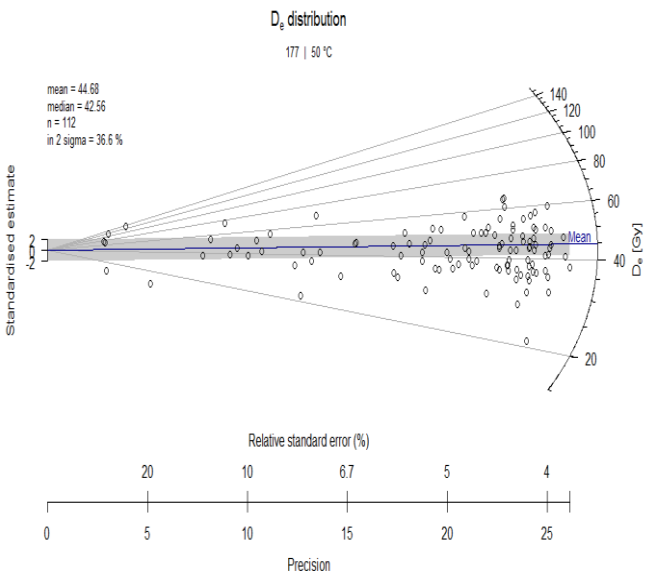

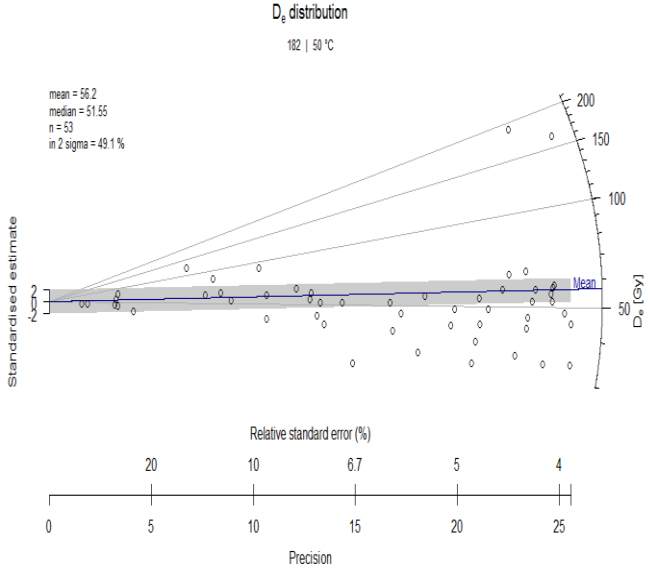

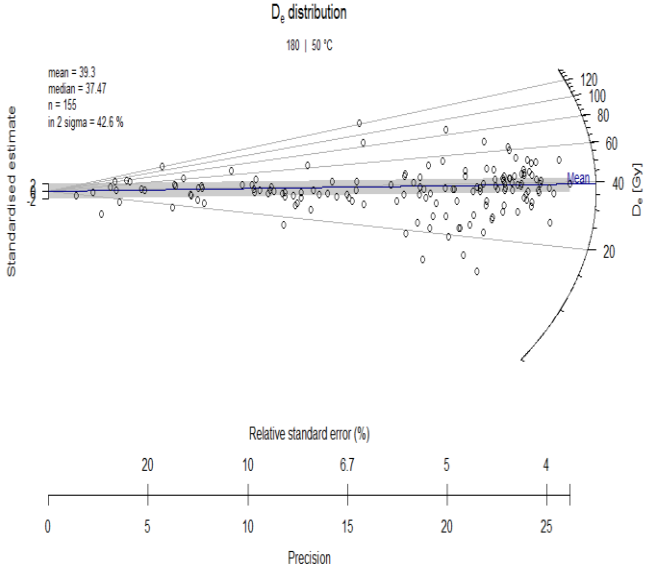

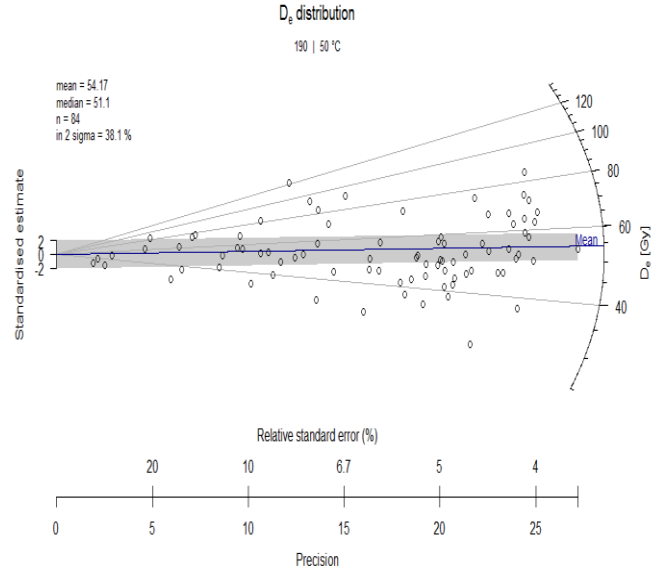

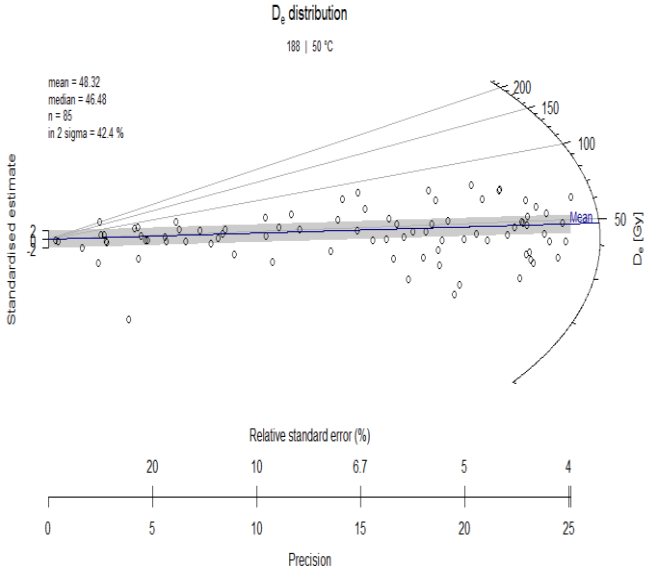

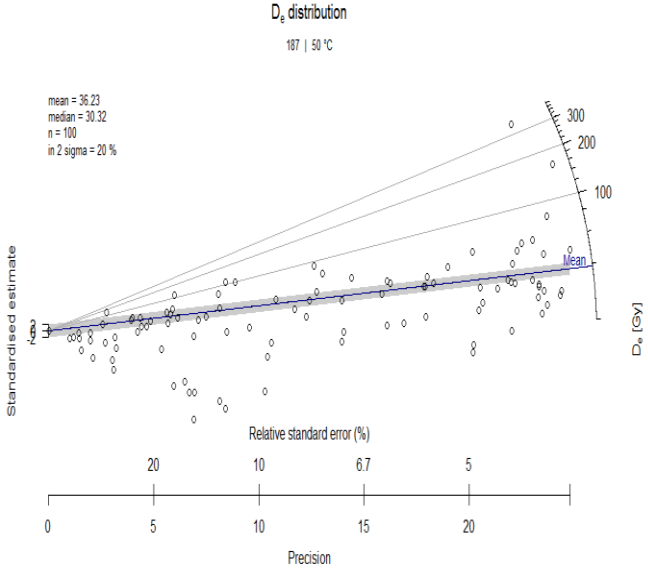

Iterated data for the 225°C measurement

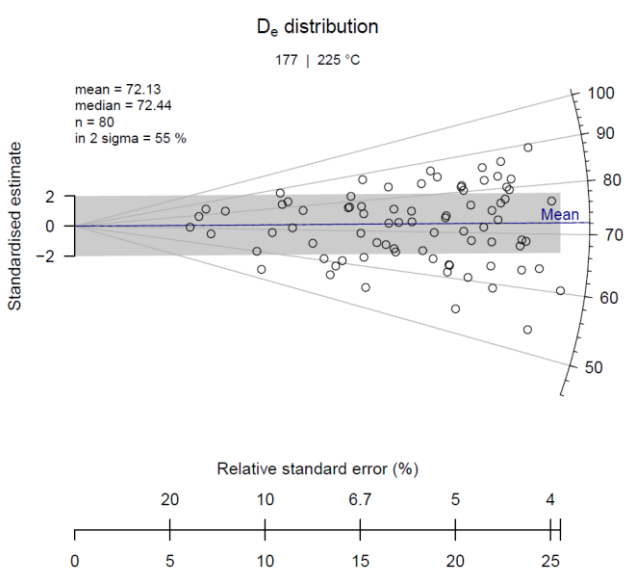

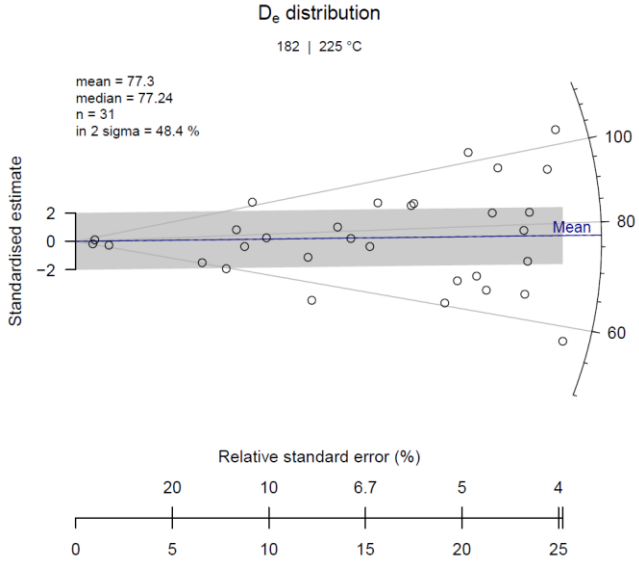

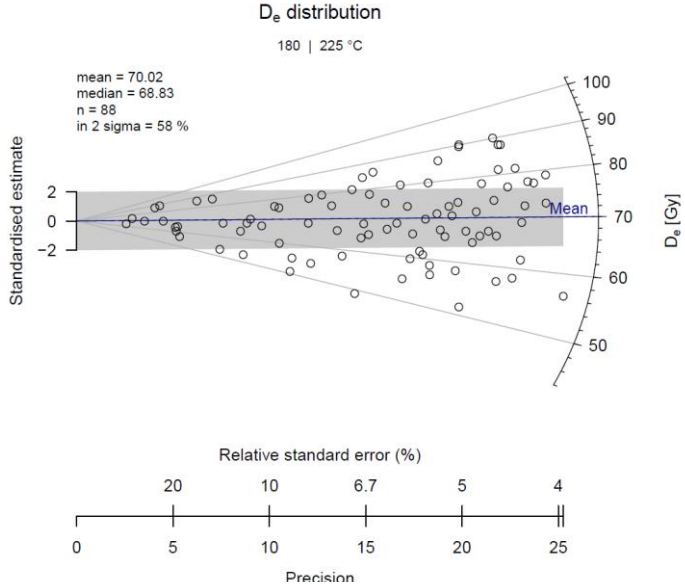

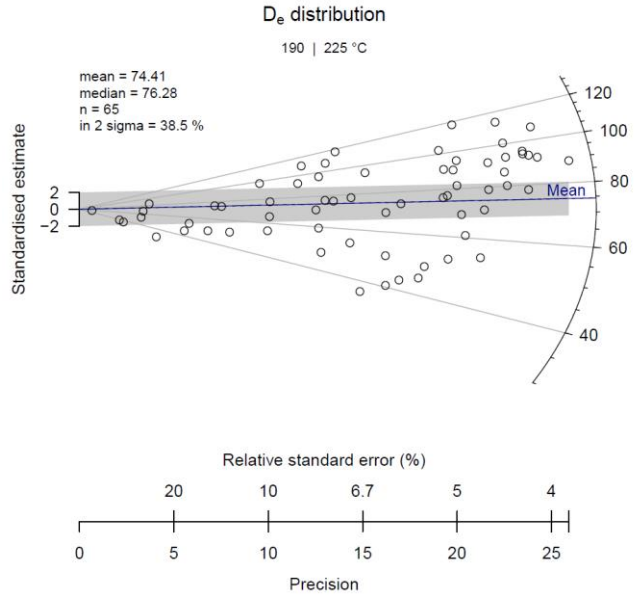

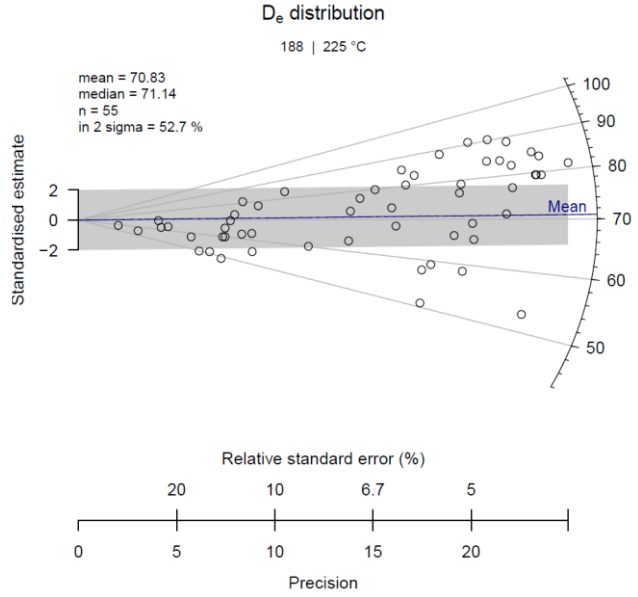

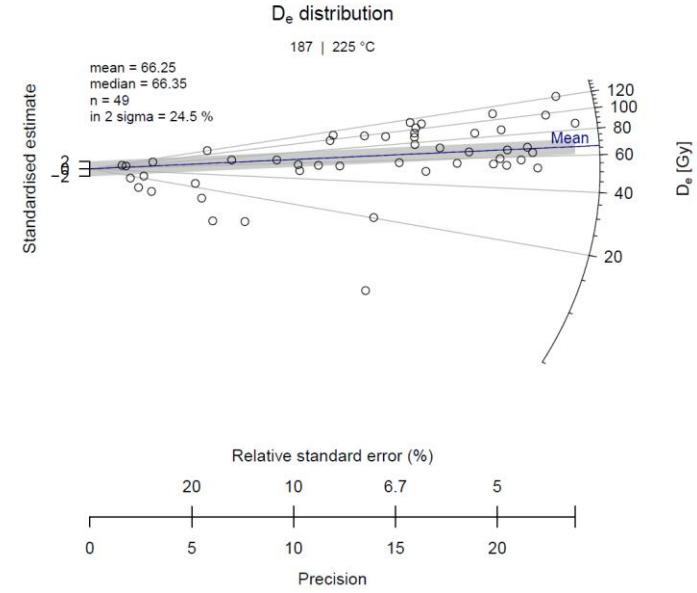

Original data for the 225°C measurement

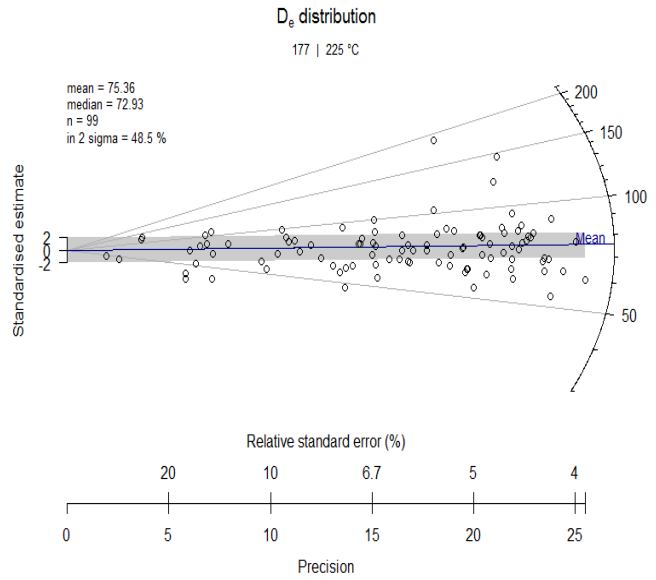

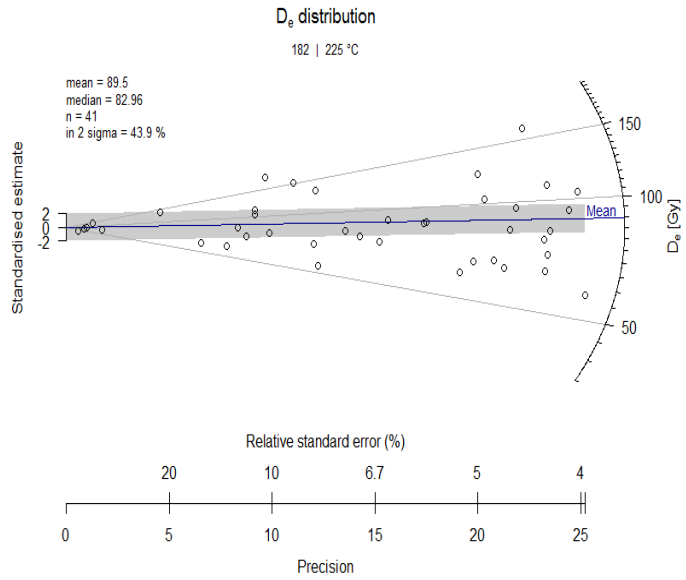

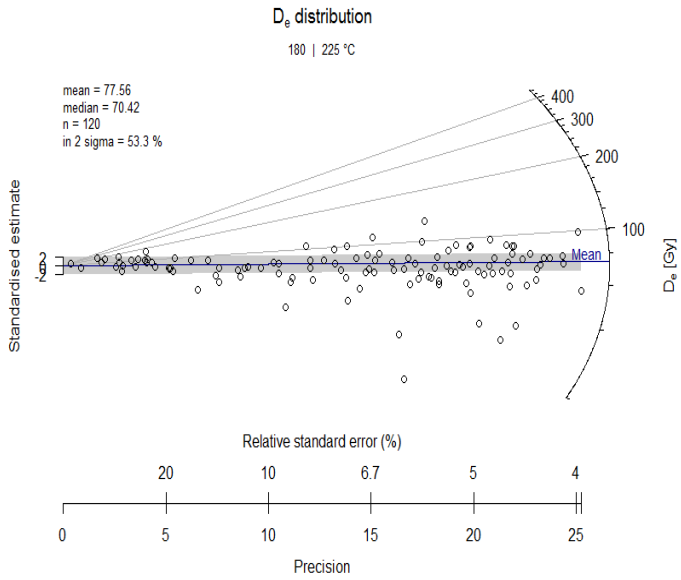

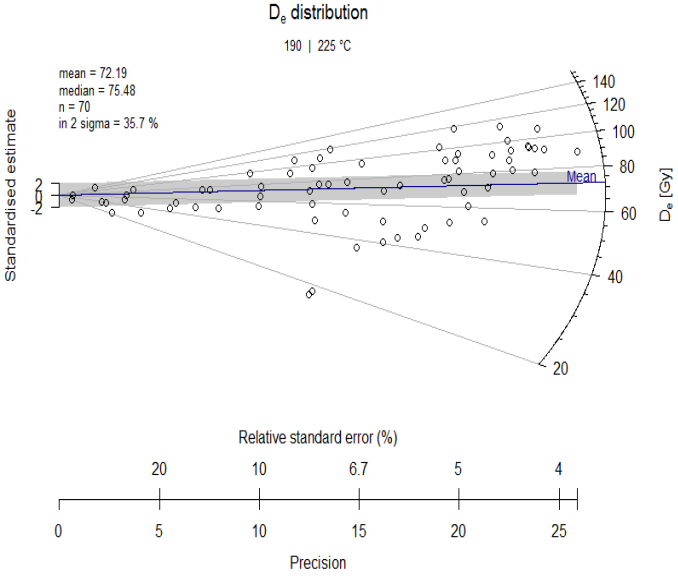

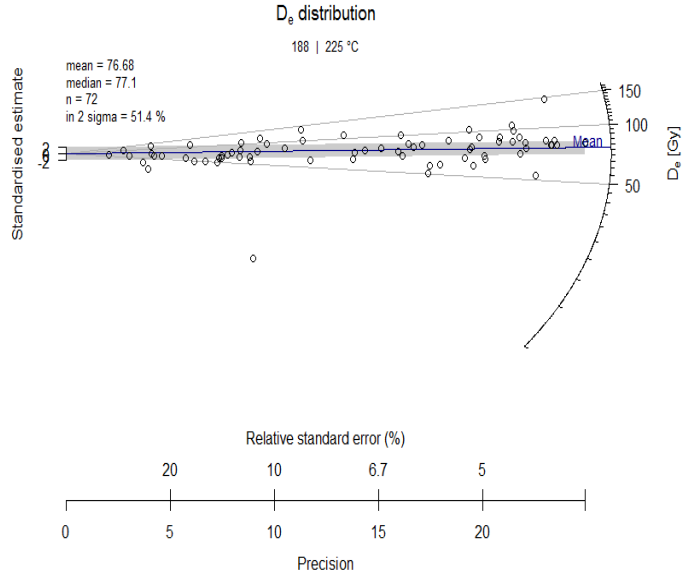

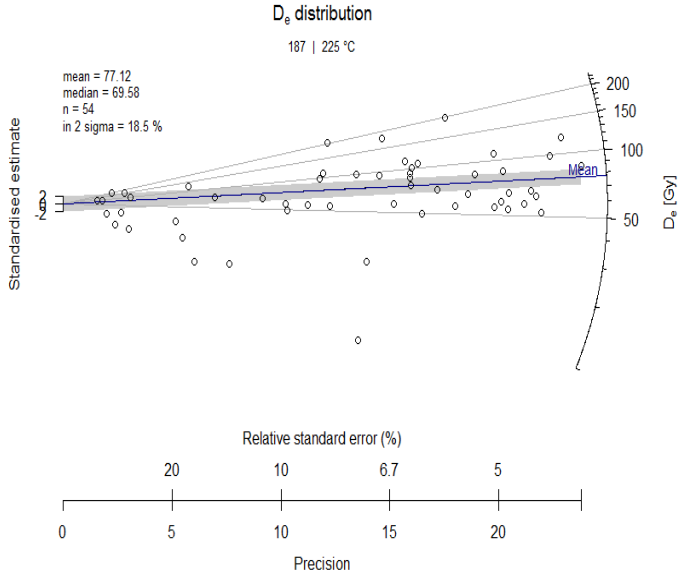

A4 Polymineral Discs

Minerals present on different samples. Discs from polymineral measurement.